APPENDIX D-2

Airflow Patterns and Pit-retention of Fugitive Dust for the Bingham Canyon Mine Study

AIRFLOW PATTERNS AND PIT-RETENTION OF FUGITIVE DUST FOR THE BINGHAM CANYON MINE

by

Ragula Bhaskar and Navin Tandon
Department of Mining Engineering
313 WBB, University of Utah
Salt Lake City, UT 84112

THE UNIVERSITY OF UTAH

A report submitted to

Kennecott Utah Copper
Environmental Affairs Department

Project Officers:
Fred Fox
Jon Cherry
Rich Borden

August 1996

ABSTRACT

A 3-dimensional finite-element numerical model was developed for analyzing the airflow patterns and pit retention of fugitive dust for Kennecott's Bingham Canyon mine, the world's largest man-made excavation. The Fluid Dynamics Analysis Package (FIDAP 7.5) was used for the study. The standard κ-ϵ turbulence model (with the near-wall approach) was used along with the Reynolds-averaged turbulent flow equations. A Lagrangian stochastic model was used to predict the particle trajectories for a given flow simulation. Sensitivity studies were conducted to perform a "what if" analysis to better understand the particle transport, dispersion and pit retention phenomena. The sensitivity to the following parameters were studied: wind speed, wind direction, atmospheric stability, source location and height, and particle size. The model predicted significantly lower values for the escape fraction of PM-10 from the Bingham pit. Escape fraction was found to be a function of different meteorological and source parameters. The escape fraction range for the various simulations conducted in the present study for the Bingham pit was found to be roughly 10-20%.

TABLE OF CONTENTS

LIST OF TABLES

LIST OF FIGURES

CHAPTER 1

INTRODUCTION

Surface mining operations (such as blasting, loading, hauling, crushing, etc.) are sources of airborne particles. The estimation of concentrations of fugitive dust/PM-10 for an open-pit mining situation has traditionally been done using Environmental Protection Agency (EPA) models such as the Industrial Source Complex (ISC) model. There is a regulatory applicability of air quality dispersion models in the review and preparation of new source permits and State Implementation Plan (SIP) revisions.

The different dust-producing operations at open-pit mines occur inside the pit, sometimes at depths of many hundreds of feet below grade. It is reasonable to suspect that only a fraction of fugitive dust generated at the pit floor escapes to the surface where it then may be transported to mine boundaries. This tendency for particulate matter to remain inside the pit has been called pit retention (TRC, 1985). There are two separate mechanisms occurring simultaneously that contribute to the pit retention phenomenon. The first is a de-coupling of the wind field in the pit from the wind field at the

surface, inhibiting or suppressing the vertical transport of particulate from the bottom of the pit to the surface. This pit retention mechanism can be expected to be most pronounced during stable low wind speed conditions, such as that occurring at night. The second mechanism by which particulate are retained is through deposition and settling on the mine pit surface and along the pit walls. It is also reasonable to expect that the presence of the mine pit would disturb the airflow above and inside the pit, so that the "plume" of dust might not have the familiar Gaussian distribution imposed by many dispersion models, or might have a significantly different trajectory which would alter plume location. Although the altered plume shape or location is technically different than pit retention, it is certainly a related issue. Until recently, most air quality models neglected the pit retention. Neglecting the plume perturbation can cause overpredictions or underpredictions, depending upon how the pit is simulated. On the other hand, if a dispersion model ignores the influence of pit retention, then the model will overpredict the downwind concentrations.

The 1990 Clean Air Act Amendments directed the EPA to analyze the accuracy of the ISC model and the AP-42 emission factors, and to make revisions as would be necessary to eliminate any significant overprediction of fugitive dust concentrations from sources such as surface mines. Historically, most air quality dispersion models

which have been used to predict particulate concentrations in the vicinity of surface mines simulated emissions as if they were released at grade level. This led to significant overpredictions in the past. The EPA's new ISC3 model (1995), with its algorithm for modeling impacts of particulate emissions from open-pit sources, considers the pit retention phenomenon and hence attempts to eliminate overprediction of PM-10 concentrations.

This chapter will examine the various investigations concerning pit retention and pit airflow which have been done in the past.

1.1 Literature Review

1.1.1 Approaches Used to Study Problems in Air Pollution

Presently, three main approaches are used to study problems in air pollution - field experiments, wind tunnel modeling and mathematical modeling.

1.1.1.1 Field experiments. Full-scale experiments, while important, are expensive and time-consuming, especially in complex terrain. Extensive measurements and analyses are required for wind, temperature and concentration distribution to gain a sufficient understanding of the fundamental physics. Generalization from field data is difficult because of peculiarities of specific sites and meteorological conditions. Controlled variation of independent variables is generally not possible, and complicating factors are abundant. However,

it is understood that field experiments can provide the "real-world" data to test the models.

Although field studies in the vicinity of surface mines have undoubtedly been influenced by pit retention, very few studies have specifically addressed pit retention. As mentioned by TRC (1985), there are two reported studies in which the investigators detected discrepancies between the measured and modeled concentrations at surface mines, and attributed the discrepancies to pit retention. After a year-long emission factor study conducted at two surface coal mines in Wyoming, it was hypothesized that only one-third of the particulate emitted in the pit was escaping. At another study conducted at the Berkeley pit in Butte, Montana, it was hypothesized that only one-half of the particulate matter emitted in the pit escaped to the surface. There is some doubt about the reliability of these two studies, as they were not specifically designed to look at pit retention, and the difference in emissions could have been caused by other errors.

One field study that specifically examined pit retention and flow fields at surface mines was the EPA funded work performed by Air Sciences, Inc., in the summer of 1983. The field data collected was reduced, analyzed and interpreted to investigate relationships between in-pit and out-of-pit parameters, as well as calculate the escape fraction/pit retention (TRC, 1985). The data had

been collected from over 800 smoke release experiments at four mines in Colorado, Wyoming and Montana. At each of the mines, smoke generators at the bottom of the pits were used to release discrete 10 second puffs of diesel fuel smoke, and these smoke releases were recorded on a video cassette recorder (VCR). An escape velocity, essentially the net upward velocity within each pit, was computed from the observed retention time of the tracers and the depth of each pit. This upward velocity, when compared to the downward settling and deposition velocity for different size particles, was the basis for the calculation of an escape fraction. The escape velocity was found to be positively correlated with wind speed and negatively correlated with the stability category. Although the study provided some important description and trends in the value of pit retention, it was understood that the computation methodology was an oversimplification of the actual phenomenon. The exact details of smoke plume trajectory or plume-ground interaction was not considered, which could be very important when the plume is very close to the pit floor and the pit walls. This simplification may cause an overestimation of the true escape fraction.

1.1.1.2 Wind tunnel modeling Wind tunnel modeling comes under the general category of physical modeling or fluid modeling. It is, in effect, the analog modeling of fluid-dynamical processes. Certain nondimensional parameters must be duplicated in the model. Due to

employment of scale models, it is actually possible to keep only some of the parameters the same or similar in both the full-scale and the wind tunnel model.

Wind tunnel modeling has been typically employed to study plants in complex terrain or to determine the effect of building turbulence on dispersion from stacks. A detailed guide (Snyder, 1981) has been published by the EPA to establish the procedures for fluid modeling. In fluid modeling, a scale model of terrain, plant, buildings, and obstructions is used. The plume rise could be simulated by using a lighter-than-air gas such as methane or helium. The surface roughness can be simulated by placing gravel or other roughness elements on the modeled floor. Fluid modeling has been found to be most effective in simulating neutral atmospheric conditions. Limited success has been achieved in modeling stable or unstable atmospheric conditions by cooling or heating the floor of the wind tunnel. In spite of its limitations, wind tunnel modeling is very important. The flow in a wind tunnel can be controlled and specific parameters can be independently adjusted. Ideally, the fluid models should be used to bridge-the-gap between the mathematical models and their applications to the field.

There is evidence in the literature that wind tunnel studies have been extensively employed to study the effect of topographical obstacles on flow and dispersion characteristics (Khurshudyan, et al., 1982; Costa, et al.,

1994).

The wind tunnel study most relevant to this project was conducted after the requirement by the Clean Air Act Amendments of 1990 to reexamine the EPA's methods for modeling fugitive particulate (PM-10) for open-pit mines (Thompson, 1994; Perry, et al., 1994). The wind tunnel study was performed at the EPA's Fluid Modeling Facility to investigate dispersion from surface coal mines (or similar sources) in support of the dispersion modeling activities. The effort was aimed at mainly assessing the ISCST2 model for applications to surface mines. In the wind tunnel study, a neutral boundary-layer approach flow with a freestream speed of 2 m/s was used for all the measurements. The study involved the measurement of steady-state, tracer-gas (ethane) concentration fields downwind of model mines of various shapes, sizes and orientations with low-momentum, point-source releases of a neutrally buoyant gas from various locations in the pit. It was assumed that due to generally high levels of turbulence in the pit, relevant information about the behavior of PM-10 could be obtained from a laboratory study using a neutrally buoyant gaseous tracer. All the model pits were rectangular and the scaling ratio was 300 to 1. The concentrations were measured using flame ionization detectors and velocity measurements were made in and around the model using a pulsed-wire anemometer. In the study, the sensitivity of downwind concentrations

to a wide range of parameters related to pit geometry and source locations were studied. The mean flow in a mine model was observed as a large vortex with the flow at the top of the mine in the direction of flow aloft. At the downwind wall of the mine, the flow was towards the mine floor. The flow moved upwind (against the direction of mean flow aloft) along the floor and then upward at the upwind face of the mine. The performance of the ISCST2 model was also assessed by comparing its results to wind tunnel results. By representing the entire opening of the rectangular pit as a surface level area source (with emissions uniform over that area), it was shown that results with ISCST2 are an overestimation over observed values. Considering the effect of recirculation phenomenon, it was stated that only the upwind edge of the model contributes to emissions. Modeling the pit using ISCST2 with an area source (a fraction of the total rectangular area), aligned with the upwind side of the actual pit demonstrated better results with slight overpredictions. Hence, it was concluded that an open pit would act as a modified area source where the emissions are greatest near the upwind side of the actual pit.

1.1.1.3 Mathematical modeling Mathematical models encompass such concepts as empirical box and statistical models, semi-empirical Gaussian plume and trajectory models, and numerical multibox, grid and particle models. Mathematical models, more generally called numerical

models, use mathematical techniques to represent the actual physical processes governing atmospheric flow dynamics and pollutant transport. Numerical models are very versatile. By making varying degrees of approximations and assumptions, numerical models can be tuned to each application. Advection by wind components, turbulent diffusion, chemical reactions, wet and dry deposition of pollutants, and other atmospheric processes can all be included in the numerical models.

Several studies utilizing mathematical modeling methodologies were found in the literature. Lee (1977) applied the finite element technique to solve the model for computing the turbulent field and diffusion in the atmospheric planetary boundary layer. Herwehe (1984) developed a 2-dimensional finite-element model to simulate the transport, diffusion and dry deposition of fugitive dust emitted from an idealized open-pit surface mine. Zhang, et al. (1993) investigated the effects of incident shear and turbulence on flows around a cubical building using a turbulent kinetic energy/dissipation (κ-ϵ) model. One of their conclusions was that turbulence in the approach flow tends to dampen the wake strength behind the building. Perdikaris and Mayinger (1995) employed numerical analysis for predicting the dispersion of continuously released neutral gases from elevated or near-ground sources in regions of complex topography.

The major advantages in using numerical models are:

the control over input data specification; and the capability to provide useful information for meteorological and air pollution scenarios in a fast, reliable and inexpensive way compared with the observational approach.

1.1.2 Surface Mine Escape Fraction Models

There are two simple equations which attempt to simulate pit retention by deriving mass escape fractions. These equations have been discussed in detail by TRC (1985).

1.1.2.1 Fabrick escape fraction. Fabrick derived a mine pit escape fraction equation that depends upon the width of the pit, the wind speed at the top of the pit and a particle size distribution:

$$\varepsilon = 1 - V_d \left[\frac{C}{u} \left(\frac{1}{2} + \ln \frac{w}{4} \right) \right] \qquad (1.1)$$

where ε is the escape fraction, u is the wind speed (m/s), w is the pit width (m), V_d is the larger of deposition or settling velocity (m/s), and C is an empirical dimensionless constant with a value of 7.

1.1.2.2 Winges escape fraction. Winges developed an equation to calculate the particulate escape fraction from surface mine pits. The escape fraction is given by:

$$\varepsilon = \frac{1}{1 + (\frac{V_d}{K_z})H} \qquad (1.2)$$

where ε is the escape fraction, V_d is the larger of deposition or settling velocity (m/s), K_z is the vertical diffusivity (m^2/sec) and H is the pit depth (m). This equation attempted to treat a very simplified dispersion scenario. Some of its assumptions were: emissions occurring at the bottom of the pit; turbulent diffusion being the only mechanism for transport of material out of the pit; and the constant eddy diffusivity assumption.

In an effort to incorporate other physical and meteorological parameters (especially wind speed) into the original Winges escape fraction equation, four alternative modifications to the Winges equation were later derived (TRC, 1986).

1.1.3 EPA's New Industrial Source Complex (ISC3) Dispersion Models

The ISC models are especially designed to support the EPA's regulatory modeling programs. These models are steady-state Gaussian plume models that provide options to model emissions from a wide range of sources that might be present at a typical industrial source complex. The ISC3 models are based on revisions to the algorithms contained in the ISC2 models. The user's guides for the ISC3 dispersion models have been published (September 1995) by the EPA, which explain user instructions and model algorithms in detail.

The ISC3 models include several new features. One of the features that has been added is an algorithm for

modeling impacts of particulate emissions from open pit sources. The ISC open pit source model can be used to simulate fugitive emissions from below-grade open pits. The ISC models allow the open pit source to be characterized by a rectangular shape with an aspect ratio (length/width) of up to 10 to 1. Since the open pit model does not apply to receptors located within the boundary of the pit, the concentrations at those receptors are set to zero by the ISC models.

The open pit model accounts for partial retention of emissions within the pit by calculating an escape fraction for each particle size category. The escape fraction for each particle size category, ε_i, is calculated as follows (EPA, 1995):

$$\varepsilon_i = \frac{1}{1 + V_g/(\alpha U_r)} \qquad (1.3)$$

where V_g is the gravitational settling velocity (m/s), U_r is the approach wind speed at 10 m (m/s) and α is the proportionality constant whose value is set as 0.029. The gravitational settling velocity, V_g (cm/sec), is calculated as:

$$v_g = \frac{(\rho - \rho_{AIR})\ g\ d_p^2\ c_2}{18\mu}\ S_{CF} \qquad (1.4)$$

where, ρ is the particle density (g/cm^3), ρ_{AIR} is the air density ($\approx 1.2 \times 10^{-3}$ g/cm^3), d_p is the particle diameter (μm), μ is the absolute viscosity of air ($\approx 1.81 \times 10^{-4}$ gm/cm/sec), c_2 is the units conversion constant (1×10^{-8} $cm^2/\mu m^2$), and S_{CF} is the slip correction factor, which is computed as:

$$S_{CF} = 1. + \frac{2x_2 \left(a_1 + a_2 \, e^{-(a_3 \, d_p/x_2)}\right)}{10^{-4} \, d_p} \qquad (1.5)$$

and, x_2, a_1, a_2, a_3 are constants with values of 6.5×10^{-6}, 1.257, 0.4 and 0.55×10^{-4}, respectively.

The variations in escape fractions across the particle sizes result in a modified distribution of mass escaping from the pit. Based on the fluid modeling (explained earlier), within-pit emissions are assumed to have a tendency to escape from the upwind side of the pit. The open pit algorithm simulates the escaping pit emissions by using an effective rectangular area source (a fraction of the entire pit opening) using the ISC area source algorithm. The shape, size and location of the effective area source varies with the wind direction and the relative depth of the pit. It is assumed that because of the high level of turbulence in the mine, the pollutant is initially mixed prior to exiting the pit.

As can be observed from the discussion above, the open pit algorithm in the ISC3 models has some strong

simplifying assumptions. The actual open pit mine could have a geometry much different than the assumption of a rectangular shape. The escape fraction equation considers very few parameters, which may not be sufficient to characterize all the complexities of the pit retention phenomenon. The calculation of effective area is based on the assumption that due to the recirculation phenomenon, emissions escape from the upwind side of the pit, which might not always be the case in the real field situation. Also, the specific heights of various emission points from the floor of the pit cannot be explicitly accounted for in the model. Although ISC3 incorporates the complex terrain screening algorithms, these cannot be applied to open pit sources.

Even with these simplifying conditions, the new ISC3 is expected to play an important role in the regulatory modeling, mainly because of ease of its use and the hardware requirements of only a PC. However, if more site-specific and accurate results are desired, advanced mathematical tools, such as finite element modeling, should be used.

1.2 Overview of the Study

Kennecott's Bingham Canyon mine is the world's largest man-made excavation: one-half mile deep and covering 1900 acres. At the top, it is nearly 2½ miles from one side of the mine to the other. Different mining

operations are sources of dust emissions in the Bingham pit. Due to the size of the Bingham pit, it can be expected that a large fraction of emitted dust will not escape the pit boundaries and will have a tendency to be retained inside the pit. This, in particular, can be expected for ground level sources deep inside the pit.

The purpose of the present study is to simulate the transport and diffusion of fugitive dust, and to quantify the pit retention/escape fraction of dust emitted in the Bingham Canyon mine. The objective is achieved through the development of a 3-dimensional finite element model. Reynolds averaged flow equations are solved to generate the turbulent flow field. Use is made of the standard κ-ϵ turbulence model and the near-wall modeling methodology. The particle transport, diffusion, and pit retention is evaluated through the use of a Lagrangian stochastic model. Sensitivity studies are then performed in order to better understand the behavior of fugitive dust under given meteorological and emission source conditions.

Chapter 2 describes the theoretical background for the Bingham pit model. The governing equations for airflow and particle trajectories, as well as some meteorological considerations are discussed. Chapter 3 discusses the steps involved in creating a 3-dimensional finite-element model. It also explains specification of input data which can be considered common to all the simulations. Chapter 4 provides detailed descriptions of

the simulation studies and presents the analyses of the results. The simulation-specific input data used to obtain the results are also discussed. Chapter 5 contains information regarding numerical validation of the model, and comparison of idealized versus actual pit geometries. Chapter 6 gives the concluding remarks with an overall assessment of the usefulness and practicality of the model and recommendations for future work.

CHAPTER 2

THEORETICAL ANALYSIS

This chapter discusses some of the theoretical aspects of the present analysis. The various motions of the air in the earth's atmosphere, from a slight breeze in the surface layer up to a general atmospheric circulation of planetary scale, are turbulent. Atmospheric turbulence plays a fundamental role in the thermal and dynamic interaction between the atmosphere and the underlying surface. Atmospheric turbulence also determines the spreading of admixtures in the air.

2.1 Turbulence Modeling

2.1.1 Mean Flow Equations

It is believed that the solution of time-dependent three-dimensional Navier-Stokes equations can describe turbulent flows completely. However, the computers are not large and fast enough yet to solve the equations directly, for the required range of length and time scales, even for simple flows (Nallasamy, 1985). Turbulent flows are represented in a majority of flow simulations by the ensemble averaged conservation equations - the so-called Reynolds-averaged equations. The mean flow equations to simulate a turbulent isothermal

flow with constant fluid properties may be presented as follows (Haroutunian and Engelman, 1991 and 1993),

Continuity:

$$\frac{\partial u_i}{\partial x_i} = 0 \tag{2.1}$$

Momentum:

$$\rho \frac{\partial u_i}{\partial t} + \rho u_j \frac{\partial u_i}{\partial x_j} = - \frac{\partial p}{\partial x_i} + \frac{\partial}{\partial x_j} \left[\mu \left(\frac{\partial u_i}{\partial x_j} + \frac{\partial u_j}{\partial x_i} \right) - \rho \overline{u_i' u_j'} \right] \tag{2.2}$$

In the above equations, u_i are the components of the mean velocity vector in the Cartesian coordinate system x_i, t is the time coordinate, p and ρ are the mean fluid pressure and density, respectively, and μ is the molecular viscosity. This formulation allows the characteristics of the mean flow to be investigated without having to resolve all the intricate details of the turbulence field. A significant drawback of this approach, however, is that unknown statistical correlation $\rho \overline{u_i' u_j'}$ enters the flow equations as a result of the averaging process. This Reynolds stress tensor represents the mean turbulent flux of momentum in the three principal spatial directions. The notation used for the Reynolds stress tensor is that prime denotes a fluctuating variable. As these turbulent fluxes are not known a priori, mathematical models are needed to approximate these in terms of mean flow

characteristics. This process is referred to as turbulence modeling. A large number of turbulence models have been explained by Rodi (1984).

2.1.2 Standard κ-ϵ Model

The standard κ-ϵ model is one of the turbulence models which has enjoyed a great deal of success. The κ-ϵ model was first proposed by Launder and Spalding (1974), and has since been universally adopted as the standard form of the κ-ϵ model. From the generalized Boussinesq eddy viscosity concept, by analogy with the laminar flow, the Reynolds stresses can be expressed as (Haroutunian and Engelman, 1993):

$$-\rho\overline{u_i' u_j'} \cong \mu_t \left(\frac{\partial u_i}{\partial x_j} + \frac{\partial u_j}{\partial x_i} \right) - \frac{2}{3} \rho \delta_{ij} \kappa \qquad (2.3)$$

where δ_{ij} is the Kronecker delta function, μ_t is the turbulent viscosity, and κ is the turbulent kinetic energy. In contrast to the laminar viscosity, μ, the turbulent viscosity, μ_t, is not a property of the fluid, but depends on the flow process.

The turbulent kinetic energy can be expressed as:

$$\kappa = \frac{\overline{u'^2} + \overline{v'^2} + \overline{w'^2}}{2} \qquad (2.4)$$

where u', v', and w' are the velocity fluctuations in the

x, y, and z directions.

The advantage of the Boussinesq's approach is that it shifts the emphasis from modeling many unknown turbulent fluxes to a single unknown μ_t. In the context of the κ-ϵ model, the expression for μ_t can be written as:

$$\mu_t = c_\mu \rho \frac{\kappa^2}{\epsilon} \tag{2.5}$$

where $c_\mu = 0.09$ is an empirical model coefficient, and ϵ is the viscous dissipation rate of turbulent kinetic energy κ. The transport equations for κ and ϵ can be written as:

$$\rho \frac{\partial \kappa}{\partial t} + \rho u_j \frac{\partial \kappa}{\partial x_j} = \frac{\partial}{\partial x_j} \left[\left(\mu + \frac{\mu_t}{\sigma_\kappa} \right) \frac{\partial \kappa}{\partial x_j} \right] + G - \rho\epsilon \tag{2.6}$$

$$\rho \frac{\partial \epsilon}{\partial t} + \rho u_j \frac{\partial \epsilon}{\partial x_j} = \frac{\partial}{\partial x_j} \left[\left(\mu + \frac{\mu_t}{\sigma_\epsilon} \right) \frac{\partial \epsilon}{\partial x_j} \right] + c_1 \frac{\epsilon}{\kappa} G - c_2 \rho \frac{\epsilon^2}{\kappa} \tag{2.7}$$

In the above equations,

$$G = -\rho \overline{u_i' u_j'} \frac{\partial u_i}{\partial x_j} \cong \mu_t \left(\frac{\partial u_i}{\partial x_j} + \frac{\partial u_j}{\partial x_i} \right) \frac{\partial u_i}{\partial x_j} \tag{2.8}$$

is the turbulence shear generation term, and the values of various constants are:

$$(\sigma_\kappa, \sigma_\epsilon, C_1, C_2) = (1.0, 1.3, 1.44, 1.92).$$

A review of simulating turbulent flows using two-equation turbulence models (including κ-ϵ) has been provided by Haroutunian and Engelman (1993). The limitation of the standard κ-ϵ model is that it is only appropriate for modeling flow regions of high turbulence levels (called high-Reynolds number regions). Another limitation of the standard κ-ϵ model is its inability to handle turbulence anisotropy.

2.1.3 Modeling of the Near-Wall Region

As mentioned earlier, the standard κ-ϵ model is not appropriate for modeling low turbulence level regions (i.e., near-wall regions adjacent to solid boundaries which contain the viscous sublayer). Another challenging aspect of turbulence modeling is that in order to resolve the sharply varying flow variables in the near-wall regions, a disproportionately large number of grid points are required in the immediate vicinity of the solid boundary. This could lead to prohibitively expensive computations.

The viscosity affected layers between the wall and the fully turbulent regions above the wall are bridged by a single layer of specialized elements. In order to accurately resolve the velocity profiles in these

elements, specialized shape functions are used. These shape functions are based on the universal near-wall velocity profile. A functional form that can be used for the velocity profile the near wall region is that due to Reichardt (as explained in Haroutunian and Engelman, 1991), which is as follows,

$$u^+ = f_R(y^+) = \frac{1}{k}\ln(1+0.4y^+) + 7.8[1-\exp(-\frac{y^+}{11}) - \frac{y^+}{11}\exp(-0.33y^+)]. \quad (2.9)$$

In this equation, k is the von Karman constant, u^+ and y^+ are the dimensionless velocity and distance which are defined as:

$$u^+ = \frac{u}{u_*} \quad (2.10)$$

$$y^+ = \frac{\rho u_* y}{\mu} \quad (2.11)$$

where u_* is the friction velocity. Reichardt's law closely matches the experimentally observed velocity profile across the viscous sublayer ($y^+ < 5$), the transitional sublayer ($5 < y^+ < 30$), and the fully turbulent layer beyond ($y^+ > 30$). It corresponds to the conditions where the near-wall flow is in local equilibrium, where the effects of streamwise variations and body forces are small and there is no transpiration at

the wall.

In the viscosity affected near-wall layers bridged by the special element layer, the standard κ-ϵ model is not solved. The variation of turbulent viscosity μ_t in the special elements is formulated by using van Driest's mixing-length model (explained by Haroutunian and Engelman, 1991). Thus, μ_t is expressed as:

$$\mu_t = \rho \ell_m^2 \left[\left(\frac{\partial u_i}{\partial x_j} + \frac{\partial u_j}{\partial x_i} \right) \frac{\partial u_i}{\partial x_j} \right]^{\frac{1}{2}} \tag{2.12}$$

where ℓ_m is the mixing length obtained from the van Driest's expression

$$\ell_m = ky[1 - \exp(-y^+/A)]. \tag{2.13}$$

In the above equation, y is the normal distance from the wall and A is an empirical constant which assumes a value of about 26 for smooth walls in the equilibrium near-wall layers. The dimensionless normal distance from the wall, y^+, is defined here in terms of turbulent kinetic energy at the top of the element, viz.

$$y^+ = \rho (c_\mu^{\frac{1}{2}} \kappa_t)^{\frac{1}{2}} \frac{y}{\mu}. \tag{2.14}$$

The computational domain for the mean momentum and continuity equation encompasses the entire flow domain down to the solid boundary, while the corresponding

computational domain for the κ and ϵ equations extends only to the top of the near-wall elements. So appropriate boundary conditions are needed at the boundary of the truncated domain for the κ and ϵ equations, and are:

$$\frac{\partial \kappa}{\partial y} = 0 \tag{2.15}$$

$$\epsilon = \frac{(c_\mu^{\frac{1}{2}} \kappa_t)^{1.5}}{ky}. \tag{2.16}$$

The viscous and buffer sublayers should be fully contained within the special near-wall elements in order for the near-wall model to function correctly.

2.2 Meteorological Considerations

2.2.1 Structure and General Characteristics of the Atmosphere

2.2.1.1 Atmospheric turbulence. Atmospheric motions come under the regime of turbulent flows. These turbulent flows are highly irregular and chaotic (random). Due to the chaotic movement of fluid parcels called turbulent eddies, an intensive mixing and transporting of heat, momentum, water vapor, and other admixtures is realized. This kind of mechanism is specified as turbulent diffusion and is analogous to the mechanism of molecular diffusion, but is much more intensive.

2.2.1.2 Planetary boundary layer. Most air pollution phenomena occur in the lower part of the

atmosphere called the planetary boundary layer, or PBL. The PBL is defined as the region in which the atmosphere experiences surface effects through vertical exchanges of momentum, heat and moisture (Panofsky and Dutton, 1984). The traditional approach is to divide the PBL vertically into various layers, each characterized by different "scaling" parameters. According to Zannetti (1990), the PBL can be divided into three major sublayers: the roughness layer, surface layer and transition (or Ekman) layer.

The roughness layer is defined as the region above the ground in which turbulence is intermittent or not fully developed, and this layer is present near the ground up to the height of the roughness length z_o. Roughly, this is the height where the wind becomes zero. The value of z_o can be obtained from standard tables or computed approximately as (Zannetti, 1990)

$$z_o = \epsilon/30 \tag{2.17}$$

where ϵ is the average height of the obstacles in the study area.

The surface layer is defined as a constant stress layer in which the fluxes of momentum, heat and moisture are assumed to be independent of height. The surface layer exists from z_o to h_s, where h_s is the height of the surface layer. For h_s, Zannetti (1990) suggests a value

of 10-200 m, while Csanady (1972) suggests 30-100 m.

The transition layer exists from h_s to z_i, where z_i varies from about 100 m to 2 km. The top of the boundary layer z_i is the lowest level in the atmosphere at which the ground surface no longer influences the dependent variables through the turbulent transfer.

2.2.1.3 Mixing height. In air pollution meteorology, mixing height is an important concept. The mixing height sets the upper limit to the dispersion of atmospheric pollutants. It is possible for pollutants released at ground level to be mixed practically uniformly up to the mixing height, but not above it (DeNevers, 1995).

2.2.1.4 Atmospheric stability. The stability of the atmosphere can be characterized as unstable, neutral and stable. There are six predominant stability classes: A, B and C represent unstable conditions, D is neutral, and E and F are stable conditions.

Neutral conditions are characterized by the presence of an isentropic (or adiabatic) vertical temperature profile in the PBL (i.e., $\Delta T/\Delta z \simeq 9.86 \times 10^{-3}$ deg/m in dry air, where T is the temperature and z the altitude). They typically occur during daytime-nighttime transitions, cloud overcasts or with strong winds (Zannetti, 1990). For flat terrain, under neutral conditions, the average wind speed shows a classical logarithmic wind profile for $z > z_o$, which is given by

$$u(z) = \frac{u_*}{k} \ln \frac{z}{z_o} \qquad (2.18)$$

where k is the von Karman constant ($\simeq 0.4$) and u_* is the friction velocity, which by definition is equal to $\sqrt{\tau_o/\rho}$, where τ_o is the stress of the wind at ground level and ρ is the air density.

Unstable conditions are typical in the daytime when maximum amount of warming of the surface and the air adjacent to the ground can take place. These conditions are characterized by the super-adiabatic vertical temperature profile and they tend to enhance the vertical air motion. Stable conditions are typical during clear nights with weak winds. These conditions are characterized by the sub-adiabatic vertical temperature profile and they tend to inhibit vertical air motion (DeNevers, 1995).

2.2.1.5 K-Theory. In the planetary boundary layer, generally, only vertical velocity gradients and momentum fluxes are important (Panofsky and Dutton, 1984). According to the classical K-Theory, the momentum fluxes are assumed to be proportional to the velocity gradients. Approximate horizontal homogeneity and stationarity are assumed in the boundary layer for the K-Theory (McBean, et al., 1979). Fluxes in the vertical direction can be formulated as (Zannetti, 1990):

$$\tau(z) = K_m \rho \frac{\partial \mathbf{u}}{\partial z} \qquad (2.19)$$

where K_m is the scalar eddy viscosity ($= \nu_t = \mu_t/\rho$), and $\mathbf{u}$ is the average horizontal wind vector.

Several models for eddy viscosity have been summarized by Panchev (1985) to explain its variability with height in the PBL. These include the step-like model, linear and power models, exponential model, and linearly-exponential model. One of the models (two-layer linear model) under neutral stratification has been explained as

$$K_m(z) = \begin{cases} ku_*z, & z \le h_s \\ ku_*h_s, & z \ge h_s \end{cases} \qquad (2.20)$$

2.2.1.6 **Surface layer**. In the surface layer, the characteristics of turbulence and the vertical distribution of mean variables are relatively simple. (Panofsky and Dutton, 1984).

As will be explained later, use can be made of the Monin-Obukhov similarity theory in the parameterization of the surface layer. One of the concepts in this theory is of Monin-Obukhov length L, the value of which can also be used in the characterization of atmospheric stability. As mentioned in Zannetti (1990), these criteria are:

$1/L < 0$ for unstable conditions

$1/L \simeq 0$ for neutral conditions

$1/L > 0$ for stable conditions.

The magnitude of L, i.e., $|L|$, describes the thickness of the layer of dynamic influence near the surface in which shear or friction effects are active participants in the physics (Azad, 1993).

Csanady (1972) explains that given a steady wind and near-neutral conditions the mean velocity distribution within the first 50 m or so from the ground is very much as in the "wall" layer portion of a two-dimensional boundary layer over a flat plate. Experimentally the logarithmic law of the wall may be verified in the "surface" portion of the PBL.

2.2.2 Wind Turbulence

In standard meteorological notation (u parallel to the mean wind, v the horizontal crosswind component, and w the vertical component), the horizontal and vertical wind fluctuations are characterized by their intensities σ_u, σ_v and σ_w, i.e., the standard deviations of the instantaneous u, v and w values, respectively. In an analysis by Panchev (1985), it was specified that

$$\sigma_f^2 = \overline{f'^2} \qquad (2.21)$$

where f could be u, v or w.

Turbulent intensities in the atmosphere depend on the

height of measurement, the roughness of the ground, and the stability of the atmosphere. Values of σ_v and σ_w are related to horizontal and vertical turbulence intensities (i_y and i_z, respectively) as follows (Zannetti, 1990):

$$i_y = \frac{\sigma_v}{\overline{u}} \quad (\simeq \sigma_\theta \text{ for small angles}) \tag{2.22}$$

$$i_z = \frac{\sigma_w}{\overline{u}} \quad (\simeq \sigma_\phi \text{ for small angles}) \tag{2.23}$$

where $\overline{u}$ is the mean wind speed at the particular height of observation, σ_θ and σ_ϕ are the standard deviations of horizontal and vertical wind direction fluctuations (for small angles, $\tan \sigma_\theta \simeq \sigma_\theta$ in radians, likewise for σ_ϕ).

2.2.3 Scaling in the Surface Layer

Many of the idealizations generally made for the PBL as a whole are more realistic in the surface layer. Principal among these are horizontal homogeneity and stationarity. In the surface layer, use can be made of Monin-Obukhov's similarity theory.

In the surface-layer theory, eddy viscosities are generally described by (Panofsky, 1975):

$$K_m = \frac{k u_* z}{\phi_m} \tag{2.24}$$

where k is the von Karman constant, u_* the friction

velocity, z the height above the ground, and ϕ_m the normalized wind shear.

The similarity theory of Monin and Obukhov introduced in 1954 allows a valid parameterization of the surface layer. According to this theory (Panofsky and Dutton, 1984), the nondimensional wind shear $\phi_m(z/L)$ is defined by

$$\phi_m(z/L) = \frac{kz}{u_*} \frac{\partial u}{\partial z} \tag{2.25}$$

where, in neutral conditions,

$$\phi_m = 1 \tag{2.26}$$

in unstable conditions

$$\phi_m = (1 - 16\ z/L)^{-1/4} \tag{2.27}$$

and in stable conditions

$$\phi_m = 1 + 5\ z/L. \tag{2.28}$$

According to Zannetti (1990), the standard deviation of the vertical wind velocity can be scaled by

$$\sigma_w/u_* = \phi_3(z/L) \tag{2.29}$$

In neutral conditions,

$$\phi_3 = constant = 1.25 \pm 0.03 \tag{2.30}$$

and in unstable conditions,

$$\phi_3 \propto 1.25(1 - 3\ z/L)^{1/3} \qquad (2.31)$$

For stable conditions, Zannetti (1990) reports that the large scatter of the data points do not allow a clear interpolation. However, according to Panofsky (1973) the ratio σ_w/u_* is invariant in neutral and stable layer. Hence for this study, σ_w/u_* for stable conditions will be approximated by the value for neutral conditions.

Additionally, Zannetti (1990) summarizes the following two relations:
In stable and unstable conditions,

$$\sigma_u = \sigma_v \qquad (2.32)$$

and in neutral conditions,

$$\sigma_u/u_* = 2.39 \pm 0.03 \qquad (2.33)$$

All the above formulations have been shown to be successful in flat terrain cases. It is expected the real surface layers (such as those on hilly terrain) will depart to some extent for the idealizations inherent in the Monin-Obukhov theory.

2.2.4 Complex Terrain

The presence of mountainous terrain introduces significant complexities in the atmospheric transport and diffusion process (Egan, 1986). Modeling air quality in

complex terrain remains a difficult task simply because of the difficulty in parameterizing the complex wind flow regimes. Dispersion in complex terrain is poorly understood, even though recent dispersion experiments and studies, such as the U.S. E.P.A. Complex Terrain Model Development Project, have allowed important parameterizations of simplified cases (e.g., dispersion near an isolated small hill and possible plume impact on it) (Zannetti, 1990).

The terrain acts to distort otherwise organized flow patterns, resulting in enhanced shear effects and turbulent eddies. This will affect the flow trajectories and ambient turbulence levels. It is realized that some simplifying assumptions become necessary while characterizing flow in complex terrain.

2.3 Particle Dispersion in Turbulent Flow

2.3.1 Two-Phase Flows

To predict particulate two-phase flows, two approaches are possible. The Lagrangian approach treats the fluid phase as a continuum and predicts the trajectories of particles in the fluid flow as the result of various forces acting on the particles. Treating the particle phase as a continuum too, and solving the appropriate equations for the fluid and particle phases makes up the basic feature of the Eulerian approach. In this study, the Lagrangian approach has been used as it

can handle particulate two-phase flows consisting of polydispersed particle size distributions. The underlying assumption in the formulation is that particle-particle interactions are neglected. The criterion for the validity of this assumption is that the dispersed phase is sufficiently dilute.

Depending on certain characteristics of the problem under examination, there are different ways the interaction between particles and turbulence can be specified. As summarized by Elghobashi (1994), the interaction will be dependent on the volume fraction of particles, which is defined as:

$$\phi_p = \frac{MV_p}{V} \tag{2.34}$$

where M is the number of particles, V_p is the volume of a single particle, and V is the volume occupied by particles and fluid. For very low values of ϕ_p ($\leq 10^{-6}$) the particles have negligible effect on turbulence, and the interaction between the particles and the turbulence is termed as one-way coupling. This means that particle dispersion, in this regime, depends on the state of turbulence. But due to the negligible concentration of the particles, the momentum transfer from the particles to the turbulence has an insignificant effect on the flow. For higher values of ϕ_p, higher-order coupling may be present in the two-phase flow.

In two-phase flows, the particles might impact with a solid wall. According to Hinds (1982), aerosol particles will attach firmly to any surface they contact, and hence exhibit characteristics different from gas molecules. But particles are known to escape collection and rebound from surfaces when impact velocity exceeds a characteristic critical velocity, which is determined by the particle size and the materials involved (Wall, S., et al., 1990). The capture of particles on impact with a surface remains an incompletely understood phenomenon. Also, it is possible for settled particles to be re-entrained in the flow.

2.3.2 Lagrangian Formulation of Two-Phase Flows

In the Lagrangian approach, the motion of each particle of the dispersed phase is governed by an equation that balances the mass-acceleration of the particle with the forces acting on it. The particles are assumed to be spherical in this analysis. Considering that only drag and gravity forces are acting on the particle, the relevant governing equation for the motion of the particle (adapted from the FIDAP Manual) is:

$$\frac{d\boldsymbol{u}_p}{dt} = \frac{(\boldsymbol{u}_f - \boldsymbol{u}_p)}{\tau} + \frac{(\rho_p - \rho_f)}{\rho_p}\,\boldsymbol{g} \qquad (2.35)$$

where $\mathbf{u}_p$ is the particle velocity, $\mathbf{u}_f$ is the velocity of the fluid, ρ_p is the particle density, ρ_f is the fluid

density, and τ is the particle relaxation time.

The parameter τ is an important term. It is a measure of the particle's responsiveness to changes in the surrounding flow field. The magnitude of the particle relaxation time, sometimes called the particle time constant, is important in understanding particle dynamics. A small particle relaxation time (relative to the time scale of the fluid) means that the particle has a chance to reach a local equilibrium with the fluid before the fluid itself has a chance to change.

τ is defined by:

$$\tau = \frac{4\rho_p D_p^2}{3\mu C_D Re_p} \tag{2.36}$$

where D_p is the particle diameter, μ is the viscosity of the fluid, C_D is the drag coefficient, and Re_p is the particle Reynolds number. The particle Reynolds number is defined by

$$Re_p = \frac{D_p \, |\boldsymbol{u}_f - \boldsymbol{u}_p| \, \rho_f}{\mu} \tag{2.37}$$

and, following Clift et al. (1978), for $Re_p < 200$,

$$C_D = \frac{24}{Re_p} \left(1 + 0.15 \, Re_p^{0.687}\right). \tag{2.38}$$

2.3.3 Particles in Turbulent Flows

Predicting the behavior of particles in a turbulent

flow is an ambitious aim. The large number of papers about the subject shows that it is hard to reach it (Ormancey and Martinon, 1984). Turbulence is the dominant mechanism for the transfer of momentum and in the absence of particle-particle interactions, it is the only mechanism which can lead to the spreading of particles.

By solving the time-averaged flow equations, the field variables obtained are the mean values. The turbulence model for the particles described via the Lagrangian approach requires some information about the fluctuations of velocities. These fluid velocity variations directly determine the extent of particle dispersion.

The typical approach for the approximation of the velocity experienced by the particle is a "random walk" model which assumes a carrier phase velocity to be the sum of a local mean velocity and random fluctuations. The random fluctuations are selected from a Gaussian distribution with zero mean and a variance related to the turbulent velocity scale coming from the model used in the mean flow solution. A stochastic approach can be used in conjunction with the κ-ϵ model which, under the assumption of isotropic turbulence, will allow the evaluation of velocity fluctuation from the turbulent kinetic energy κ obtained as field variable from the solution of the flow problem:

$$u' = \lambda(\frac{2}{3}\kappa)^{\frac{1}{2}} \tag{2.39}$$

where λ is the random generated number sampled from a normal distribution (between 1 and -1). Information about the frequency of the fluctuation sampling is also required to model the particle-eddy interactions. For this purpose, the "eddy lifetime" concept, initially developed by Gosman and Ioannides (1981) is used. Based on the local kinetic energy κ, and dissipation ϵ, an assumed eddy length, L_e, is computed:

$$L_e = C_\mu^{3/4} \frac{\kappa^{3/2}}{\epsilon} \tag{2.40}$$

and the eddy lifetime, t_e, is computed by

$$t_e = \frac{L_e}{(\frac{2}{3}\kappa)^{\frac{1}{2}}}. \tag{2.41}$$

The transit time, t_t, is also computed to account for the possibility that the particle can leave the eddy before the end of eddy lifetime.

$$t_t = -2 \ln\left(1 - \frac{L_e}{\tau\,|\boldsymbol{u}_f - \boldsymbol{u}_p|}\right) \tag{2.42}$$

where $|\mathbf{u_f} - \mathbf{u_p}|$ is the relative velocity at the start of the interval. During the computation of trajectories, whenever an interval of time equal to the minimum of t_e or

t_t is elapsed, it is assumed that the interaction with a new eddy has begun and a new fluctuation is sampled. During computation of t_t, if $L_e > \tau \, |\mathbf{u}_f - \mathbf{u}_p|$, then the interaction time is always taken to be t_e. This technique ensures that the information about the particle-turbulence interactions are not lost.

CHAPTER 3

MODEL DEVELOPMENT

In this chapter, the information and processes necessary to create the 3-dimensional Bingham pit model are discussed. FIDAP 7.5 (Fluid Dynamics Analysis Package) was used for the analysis. The model was developed and the simulations were generated using the Silicon Graphics Power Challenge XL supercomputer housed at the Utah Supercomputing Institute. The steps involved in the model development include specifying:

- 3-dimensional geometry and finite element mesh generation
- boundary and initial conditions
- model definition data and control information.

After the model was developed, the simulations were generated and the results of airflow patterns and particle trajectories were analyzed. The details of model development and execution are explained in FIDAP manuals (Fluid Dynamics International).

3.1 Geometry and Finite Element Mesh Generation

In order to perform a computer simulation of the problem, it is necessary to create a model of the flow

domain. This involves two distinct phases - description of the geometry of the flow domain, and generation of a finite element mesh.

3.1.1 Geometry Definition

The geometry for the Bingham Canyon mine was defined using a contour map (1" = 1000' scale), marked with a photo date of 7-5-95. In order to study the airflow patterns and pit retention of fugitive dust, it was essential that the model covers the pit as well as the surrounding area. This area was determined to be 23,000 feet (North-South) by 20,000 feet (East-West). It should be noted that the directions refer to the true directions, and not the mine directions.

The geometry definition process is illustrated in Figure 3.1. The X-axis points in the direction of TE (True East) and the Y-axis points in the direction of TN (True North). The Z axis points vertically upward. A grid comprised of several North-South parallel lines was placed on the contour map (actual 1"=1000' scale map) and several points were chosen on each line. The map was digitized using AUTOCAD to generate (X,Y) pairs of points and the Z-coordinate was read by interpolating between the contour intervals. There were enough numbers of points chosen to represent the complex terrain effectively. Using the defined points in FIDAP, order-3 curves were created and subsequently a rectangular surface (in plan

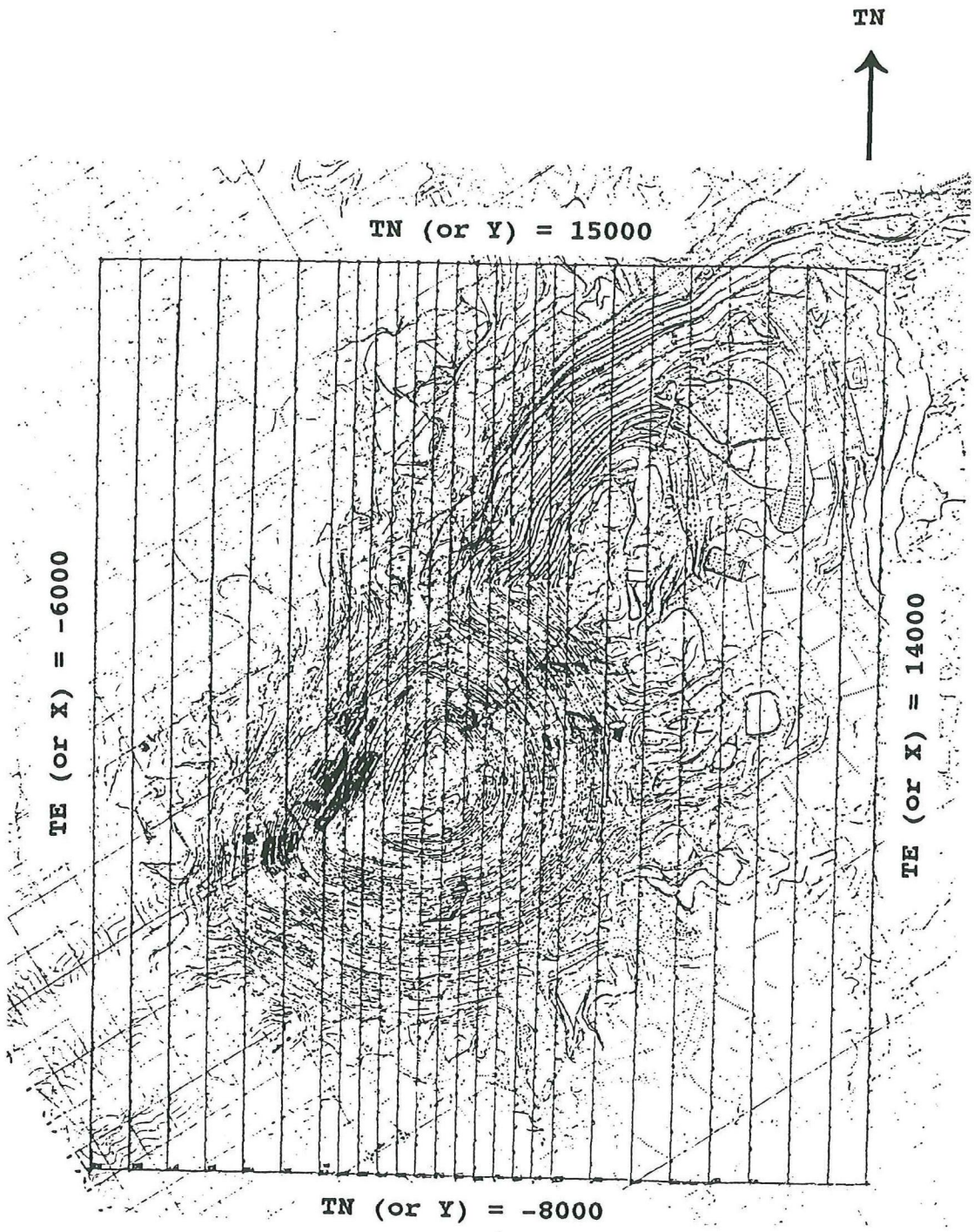

Figure 3.1 Bingham Canyon Mine Geometry (reduced in size from the 1"=1000' scale map).

view) was generated which represents the lower boundary of the domain.

3.1.2 Mesh Generation

After the geometry of the ground surface was defined, a mapped mesh was created on the surface. This mapped mesh consists of 4-node linear elements.

The upper boundary of the domain was specified using the study by Draxler and Heffter (1981). In that study, the height of the mixed layer was determined from the rawindsonde (air sounding) data collected over a five-year period at 70 stations throughout the U.S. The annual average value of the mixing depth for Salt Lake City was specified as 2959 m (9705.5 ft). With the elevation of ground as 4221 feet (from Local Climatological Data, Salt Lake City), the average mixing height was calculated as 13,926.5 feet above mean sea level (AMSL). It is recognized that the mixing height varies diurnally and seasonally, and will be affected by the presence of the Oquirrh mountains. However, this data was chosen due to the lack of better data.

After the upper boundary had been specified, the mapped mesh generated on the ground surface was projected in the Z-direction to generate a 3-dimensional finite element mesh composed of 8-node linear elements. The grading of the mesh was changed from fine to coarse in the Z-direction. This is appropriate as large gradients of

variables are not expected at higher altitudes.

The mapped mesh generated on the ground surface is illustrated in Figure 3.2 and the 3-dimensional finite element mesh for the entire computational domain is illustrated in Figure 3.3. In all, there are 19,872 nodal points and 22,862 3-dimensional elements in the domain.

3.2 Boundary and Initial Conditions

A steady-state flow field is required first in order to compute the time dependent particle trajectories. Appropriate boundary conditions are needed to be specified at all the boundaries of the computational domain. The six faces which define the domain for the Bingham Canyon mine were named "north", "south", "east", "west", "top", and "bingham". The entity names "north", "south", "east", and "west" refer to vertical faces of the domain, "top" refers to the mixing height, and "bingham" refers to the ground at the mine and surrounding areas. The location of these six faces has been shown on figure 3.2.

Since the κ-ϵ turbulence model is being used, appropriate boundary conditions have to be prescribed for κ and ϵ, along with those for the three components (u_x, u_y, u_z) of velocity. The boundary conditions for the variables are assigned in the following manner.

Inlet planes: Inlet planes refer to planes from where the wind enters the domain. For instance, in the case of northerly winds, the face "north" is the inlet

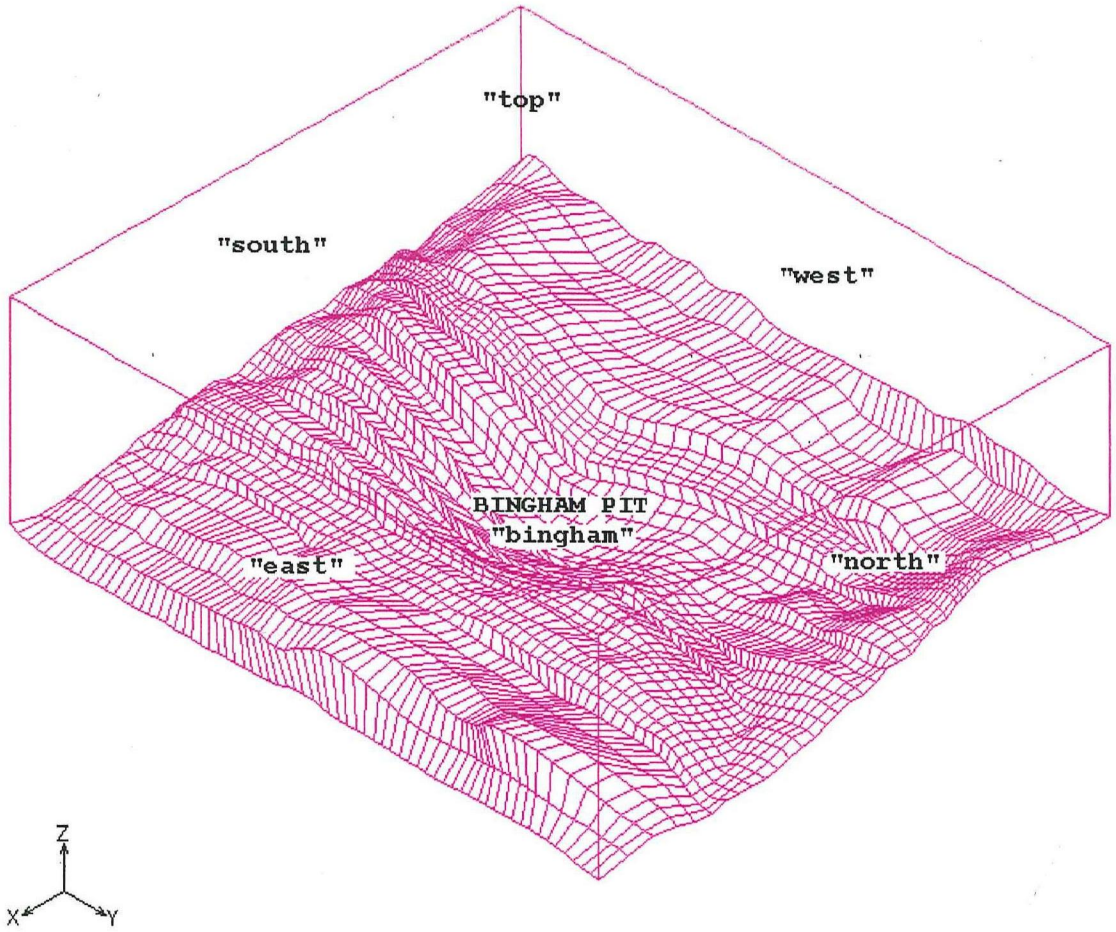

Figure 3.2 Two-dimensional mesh on the ground surface

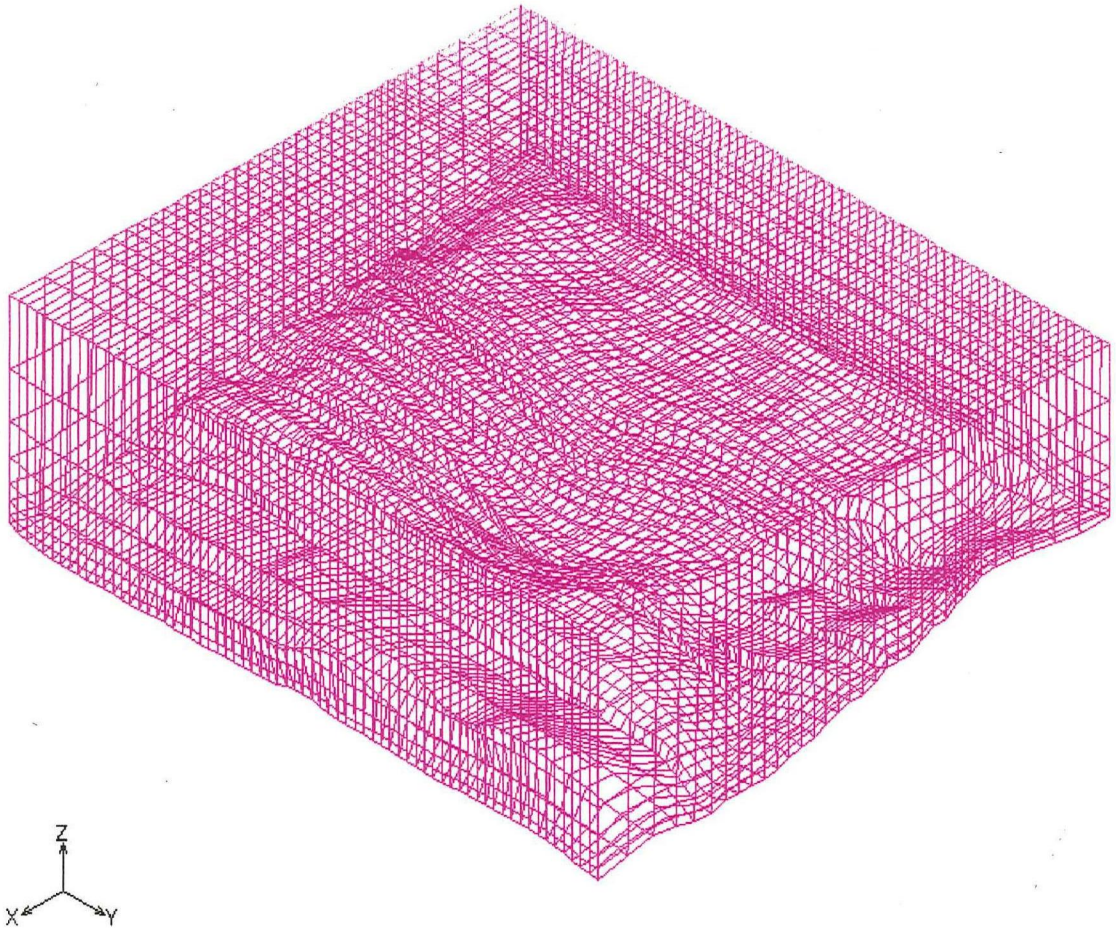

Figure 3.3 Three-dimensional mesh in the computational domain

plane. Dirichlet (i.e., prescribed or essential) boundary conditions are applied to all the variables at an inlet plane. Values for u_x, u_y and u_z are assigned based on the wind speed and direction. The value for the turbulent kinetic energy κ is calculated based on the wind speed and the stability of the atmosphere. The value of the eddy viscosity (ν_t or K_m) is also computed and the dissipation at the inlet plane is specified by $\epsilon = C_\mu \kappa^2/\nu_t$. The specific values used for the simulations will be specified when individual cases are discussed. Strictly speaking, the values prescribed should ideally be obtained from experimental measurements. It is however recognized that such experimental data is rarely available for typical simulations.

Symmetry planes: At the symmetry planes, all gradients normal to the plane and the normal velocity itself are set to zero. In the computational domain for Bingham Canyon mine, the entity "top" is a symmetry plane. At this plane, u_z (vertical component of velocity) is set to zero. As a part of the finite element discretization, the zero-gradient condition is automatically applied if no other boundary conditions are explicitly specified.

Outlet planes: Outlet planes are those through which the wind leaves the domain. For example, in the case of northerly winds, the entities "south", "west" and "east" are outlet planes. The gradients of all the variables normal to the outlet plane are set to zero. The location

of an outlet plane should be sufficiently far from regions of the flow where large perturbations occur in the flow field.

Walls: At the wall (ground surface), all components of velocity are set to zero to satisfy the no-slip boundary condition. The near wall methodology (explained earlier in Chapter 2) is invoked in the near-wall region.

In order to improve the convergence characteristics of the κ-ϵ runs, nonzero initial guess fields are used for the variables. The values prescribed at the inlet plane are used as initial conditions for the entire domain.

3.3 Model Definition Data and Control Information

Equations Solved: The model is a 3-dimensional model which considers air to be incompressible and a Newtonian fluid. Isothermal conditions were assumed for the purposes of generating the simulations. The standard κ-ϵ turbulence model was used for the simulation of flows. One of the limitations of the κ-ϵ model is that it is isotropic.

Solution Approach: In solving the flow equations numerically, a highly nonlinear set of equations are being solved. Invoking the κ-ϵ turbulence model entails the solution of two additional transport equations. This can significantly increase the CPU requirements of the numerical solution. Moreover, the introduction of the κ and ϵ equations significantly increases the nonlinearity

and coupling of the overall flow equations and this, in general, acts to destabilize the convergence characteristics of the numerical solution. For the numerical solution of the problem, the "Segregated" solver (FIDAP Manuals) using direct Gaussian elimination was used. The Segregated solver creates a set of equations for a single degree of freedom at a time and cycles sequentially through all unknowns at each iteration. Compared to so-called fully-coupled solvers (which solve all unknowns at the same time), the Segregated solver requires significantly less computer memory and disk storage to perform a solution to a given large problem. During the iteration process, the convergence criterion to be satisfied is:

$$\frac{\|\boldsymbol{U}_i - \boldsymbol{U}_{i-1}\|}{\|\boldsymbol{U}_i\|} \leq DTOL \qquad (3.1)$$

where $\|.\|$ is a root mean square norm. The vector **U** comprises of all the nodal values of a particular degree of freedom. The convergence criterion is checked for each degree of freedom, i.e., three components of velocity (u_x, u_y and u_z), pressure, turbulence kinetic energy, and dissipation. Convergence is considered to be obtained when the criterion is met for all degrees of freedom. The recommended value of the DTOL tolerance is 0.001.

Fluid Properties: The viscosity μ of the air was set to 1.8×10^{-5} Pa-sec (1.21×10^{-5} lbm/ft-sec). Normally

the density (ρ) of air is specified as 1.2 kg/m^3 (at 1 atm pressure and 20°C). But due to higher altitudes, the use of the value of 1 kg/m^3 (6.25 x 10^{-2} lbm/ft^3) seemed more appropriate.

3.4 Model Execution

After the model was created (geometry and mesh generation, specification of initial and boundary conditions and, finally, entering the model definition data and control information), the model was run on the Utah Supercomputing Institute's Silicon Graphics Power Challenge. The Power Challenge is a 12 processor shared memory computer that has 2 Gbytes of 4-way interleaved core (RAM) memory, and 12 Gbytes of disk space.

A typical model run consumed about 70-80 hours of CPU time, which by conventional standards, is a extremely large computer usage time.

3.5 Particle Characteristics and Trajectories

Due to an extremely small volume fraction of particles with respect to the volume of the carrier phase (air) in the pit, the assumption of one-way coupling is reasonable. This means that while the dynamics of the carrier phase drives the motion of the dispersed phase (particulate), the presence of the dispersed phase has no effect on the dynamics of the carrier phase. Because of the one-way coupling in the model, it was possible to solve the problems in sequence, i.e., first the flow field

for the carrier phase was solved, and then the particle dynamics equations were solved based on the flow field computed earlier.

For the particle dynamics, the Lagrangian formulation was used. The drag, as well as the gravity forces, were included in the computations. The particles were introduced at desired locations in the domain and were then tracked as they interacted with the turbulence in the flow field. EPA refers to emissions in terms of aerodynamic particle sizes, therefore a unit density (1 g/cm^3) was assigned to the particles. Since the κ-ϵ model was used for the flow fields, several particles were introduced at each location, and the stochastic model (explained earlier in Chapter 2) was used to track the particles through the domain. Individual trajectories of the particles having the same initial attributes differed because of the turbulent nature of the flow.

Information had to be specified regarding the interaction of particles if they came in contact with a boundary of the computational domain. This interaction could be that the particles escape, rebound or remain trapped when they come in contact with the domain boundary. The "escape" condition means that when the particle exits the domain, it carries with it its mass and momentum. The "rebound" condition means that the particle exchanges momentum with the boundary. The exchange of momentum is determined by the value of the restitution

coefficient. A restitution coefficient less than one would imply that the particle lost some momentum to the wall. For the "trap" condition the particle velocity becomes zero at the wall, and the particle loses its entire momentum to the wall. In the simulations generated for the Bingham Canyon mine, the entities "north", "south", "east", and "west" were specified as "escape" boundaries, "bingham" (ground surface) was specified as a trap boundary and "top" was specified as a "rebound" boundary with a restitution coefficient of 1.

The details of the particle characteristics, including the particle sizes, emission points, number of trajectories, etc., will be specified when the individual cases of simulation studies are discussed.

CHAPTER 4

SIMULATION STUDIES AND ANALYSIS OF RESULTS

4.1 Choice of Simulations

Unlike many manufacturing plants, the mode of operation of a mine is highly variable, and so are its dust emissions. The relative amounts of ore and overburden mined can vary tremendously. Haulage of ore and waste is the largest single source of dust emissions at the Bingham Canyon mine. The location of the dust emissions depends on where the material is being mined, handled or hauled. Along with the variability in the emission sources, the meteorological parameters are also highly variable. These meteorological parameters are wind speed, wind direction and atmospheric stability. Also, the features of the local terrain may have some critical effects on the impacts of emissions.

Because of almost infinite possible combinations of various source characteristics and meteorological parameters, it would be almost impossible to model all the cases. Perhaps it would be more feasible to study the effects of individual parameters. In this study, the simulations were planned so that the "sensitivity analyses" could be conducted. In this scheme of work,

only one parameter at a time could be altered, keeping all other parameters constant. Thus, meaningful conclusions could be drawn about the effects of the parameter on the dispersion and pit retention of dust.

Site-specific data was analyzed in order to prepare the input data to generate the simulations. Wind rose data collected at 6290 level Mine Office for the year 1994 was analyzed to determine most frequent wind directions. One such wind rose (for January 1994) is presented as Figure 4.1. It was determined that the northerly, north-easterly and north-westerly winds were more frequent, with the frequency of northerly winds the highest. Winds from other directions were present, but their frequencies were lower. Also, the mine environmental data from the period May 1994 to May 1995 was examined for the range of wind speeds. The wind sensor was about 15' high above the ground level. One such wind speed data (for July 1994) is presented as Figure 4.2. In general, while the average speed range was typically 1 to 10 miles/hour, a peak gust could even be higher than 50 miles/hour.

The site-specific wind speed and direction data was used to make the simulations more representative of the actual conditions. For instance, because of the very high frequency of the northerly winds, the wind direction was set as northerly in all cases, except when the effect of wind direction had to be evaluated. Likewise, because of a typical wind speed range of 1 to 10 miles/hour, wind

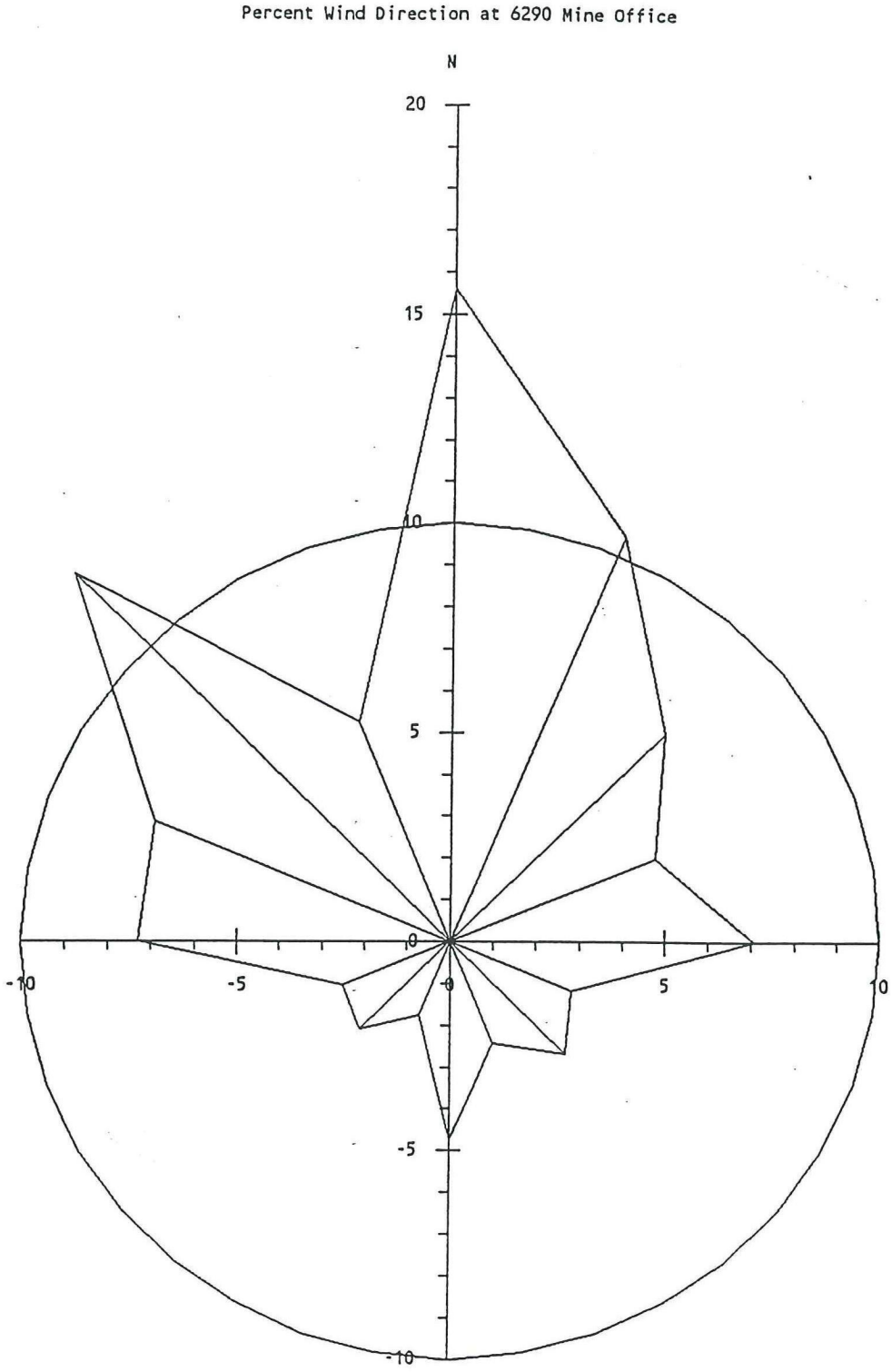

Figure 4.1 Wind rose for January 1994

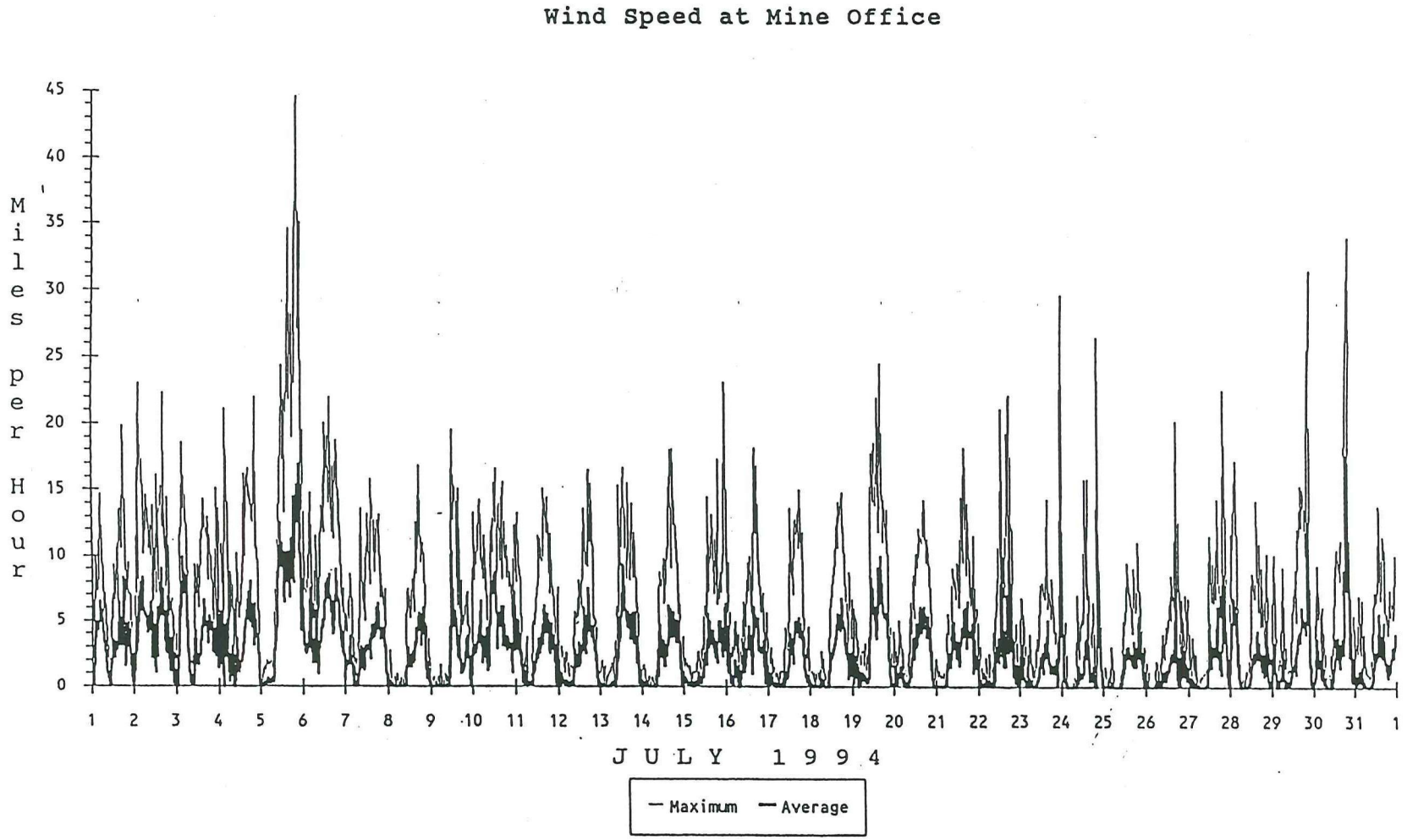

Figure 4.2 Wind speed data for July 1994

speed was set to 6 miles/hour (in the mid-range) in all cases, except when the effect of wind speed had to be evaluated. The turbulence or stability data was not available. So neutral stability (D) was used in all cases, except when the effect of stability had to be evaluated.

It was decided that nine "flow" situations would be enough to present a representative profile of the meteorological conditions. These nine cases are tabulated in Table 4.1. To study the effects of emission source characteristics, it was decided that a wind speed of 6 miles/hour, northerly wind direction and neutral stability would be used.

4.2 Specification of Input Data

This section discusses the specification of input data which was required to generate the individual simulations. The data explained here is supplementary to general input data explained in Chapter 3.

4.2.1 Wind Profile

An important characteristic of wind is the variation of speed with height. The wind speed is zero at the surface, and it increases with height above ground, up to the top of the atmospheric boundary layer. Above this layer, gradient wind exists, which does not vary with height. Either a classical logarithmic profile (Equation (2.18)) or a simple power-law is generally used to

Table 4.1 Simulation Cases

Case Number	Wind Speed (miles/hour)	Wind Direction (coming from)	Atmospheric Stability
1	6	north	D (neutral)
2	6	north	A (extremely unstable)
3	6	north	F (moderately stable)
4	2	north	D (neutral)
5	10	north	D (neutral)
6	30	north	D (neutral)
7	6	south	D (neutral)
8	6	west	D (neutral)
9	6	east	D (neutral)

describe the wind variation with height. However, these empirical formulas are valid for speed variation over flat (horizontal) areas. For the complex terrain in the Bingham Canyon area, use of these formulas as boundary conditions (for the upstream boundary of the domain) is not appropriate simply because of the complex wind flow regimes that might be present.

In the Bingham pit model, the boundaries were chosen to be sufficiently far from the area of interest, and a uniform profile was used to describe the wind on the upstream boundary. The assumption was that because of the no-slip boundary condition assigned to the ground, the wind would adjust to an appropriate profile depending on the terrain, before the flow reaches the area of interest (the emission points).

4.2.2 Turbulent Kinetic Energy κ and Dissipation ϵ

This section discusses the values of turbulent kinetic energies and dissipation which were used as upstream boundary conditions to generate various simulations. The values of κ and ϵ govern the turbulence structure of the atmosphere. As mentioned earlier, ideally these values should be obtained from field or experimental measurements. These measurements were not available in this study. Since the primary objective of this study was a comparative analysis of different meteorological and source parameters, it was considered

appropriate to calculate the values of κ and ϵ based on formulations that exist in the literature. All the necessary formulations have been explained in Chapter 2.

Table 4.2 presents the wind fluctuation data that was used. The data has been adapted from Tables 7-1 and 7-2 of Zannetti (1990), where he tabulates the wind fluctuation data in order to classify different stability categories. The footnotes of the tables explain that the data presented was for steady-state conditions, a measurement height of 10 m, for level terrain, and an aerodynamic surface roughness length of 15 cm. Because of lack of better data, use of this data was considered appropriate for the Bingham pit model.

For the calculations, values of the Monin-Obukhov length L were also required for different stability categories. The following power law function was used to characterize L (Zannetti, 1990)

$$1/L = az_o^b \qquad (4.1)$$

where a and b are constants, and z_o is the roughness length in meters. Table 4.3 provides the values of constants a and b. Using Equation (2.17) and the height of obstacles (pit benches) as 50 feet (or 15.2 m), the value of z_o was specified as 0.5 m. Based on the values of a, b and z_o, values of L were calculated for each stability category.

Table 4.2 Wind fluctuation data (adapted from Tables 7-1 and 7-2 of Zannetti, 1990)

Pasquill Stability Category	Standard Deviation of the Horizontal Wind Direction Fluctuations (σ_θ)	Standard Deviation of the Vertical Wind Direction Fluctuations (σ_ϕ)
A	25°	12.2°
D	10°	6.4°
F	2.5°	1.5°

Table 4.3 Coefficients a and b to calculate Monin-Obukhov Length (adapted from Table 3-4 of Zannetti, 1990).

Stability Class	a	b
A	-0.0875	-0.1029
D	0.	0.
F	0.03849	-0.1714

As explained earlier, several models for eddy viscosity (K_m or ν_t) have been proposed in the literature. One such model was mentioned earlier by Equation (2.20). During simulation of the LNG (Liquified Natural Gas) vapor spread and dispersion by finite element methods, Chan, et al. (1980) used the eddy viscosity values of 0.1, 1 or 10 m^2/sec to represent different atmospheric conditions. Yu (1977) examined several parameterization schemes for the vertical turbulent exchange processes in the atmospheric boundary layer. One of the parameterizations examined by Yu was a constant eddy viscosity model where K_m was set constant from the top of the constant flux layer (surface layer) throughout the entire boundary layer. His conclusion was that a constant eddy viscosity model performs quite well near the lower levels, but becomes less satisfactory at higher levels. In the Bingham pit model, since the emissions take place near the ground level, it was important to characterize the lower levels as accurately as possible. The values of eddy viscosities were calculated at the top of the surface layer (assumed 70 m) and were used to assign the upstream boundary conditions of turbulent kinetic energies κ and dissipations ϵ.

Calculations for κ and ϵ: Calculations were done for the nine test cases tabulated in Table 4.1 and the values were used as prescribed boundary conditions on the upstream boundary. For a given stability category, σ_θ and

σ_ϕ were obtained from Table 4.2. For a given wind speed, σ_v and σ_w were calculated by the expressions (2.22) and (2.23) (using $\tan \sigma_\theta \approx \sigma_\theta$, likewise for σ_ϕ). Next, the value of u_* was computed using the relations (2.29), (2.30) and (2.31). The value of σ_u was then obtained through Equations (2.32) and (2.33). Knowing the values of σ_u, σ_v and σ_w, the value of turbulent kinetic energy κ was calculated from (2.4) and (2.21). Next, the value of ϕ_m was computed from (2.26), (2.27) and (2.28), and then the value of K_m (or $\nu_t = \mu_t/\rho$) was calculated using Equation (2.24). Knowing K_m and κ, ϵ was estimated using Equation (2.5).

The values of κ and ϵ computed and used in the simulations are listed in Table 4.4.

4.3 Sensitivity Studies and Analyses

One of the major objectives of the Bingham pit modeling study was to provide the basis for developing a better understanding of the release of dust from the pit and the sensitivity of the dust dispersion and pit retention to a wide range of meteorological and source parameters. In this study, the analysis was conducted to understand the sensitivity to:

- wind speed
- wind direction
- atmospheric stability
- source location and height

Table 4.4 Values of computed turbulent kinetic energy κ and dissipation ϵ.

Wind Speed ft/sec (mi/hr)	Stability Category	Simulation Case(s)	Turbulent Kinetic Energy κ (ft^2/sec^2)	Dissipation ϵ (ft^2/sec^3)
8.8 (6)	A	2	18.6378	1.0892×10^{-1}
8.8 (6)	D	1,7,8,9	3.4703	1.4952×10^{-2}
8.8 (6)	F	3	0.174	2.6068×10^{-3}
2.93 (2)	D	4	0.3856	5.5262×10^{-4}
14.67 (10)	D	5	9.6391	6.9214×10^{-2}
44.0 (30)	D	6	86.7512	1.8684

- particle size

The sensitivity analysis for each parameter involves either individual cases or combination of cases outlined in Table 4.1. These cases will be referenced by number in the analysis.

As mentioned earlier, a stochastic model for particles was used because of the turbulent nature of the atmosphere. To evaluate the results of the stochastic model, a number of particles were introduced at a dust emission point and their trajectories were tracked through the time. The particles were tracked in 10 seconds increments. Due to the turbulence, different particles with the same initial conditions could have different trajectories and dispersion. This required introduction of a very large number of particles at each emission point. After a few test runs, it was concluded that 500 particles (all of the same size) introduced at each dust source location would yield consistent results. Since the total massflow could be divided equally among the 500 particles, the fraction of the total number of trajectories escaping the domain boundaries could be used as a measure of escape fraction. Thus, the escape fraction ε can be computed as

$$\varepsilon = \frac{n}{N} \, x \, 100\% \qquad (4.2)$$

where n is the number of trajectories leaving the domain

and N is the total number of trajectories (500). If desired, the pit retention could be calculated as (100-ε)%.

As tabulated in Bingham Canyon Mine Emission Inventory (1994), a majority of PM-10 emissions (70-75%) are due to haul roads. It is clear that near-ground level sources such as haul roads are the major contributors of dust emissions. Hence, greater emphasis was placed on these sources in this study. In the model evaluation protocol for modeling fugitive dust impacts from surface coal mining operations, the EPA (1994) suggested a release height of 2 m to be used in representing haul roads. The release height of 2 m approximates the level in the dust plume that equally divides the mass flux. In the Bingham pit study, a release height of approximately 7 feet above the ground was used for representation of ground-level sources.

4.3.1 Sensitivity to Wind Speed

Four cases (4,1,5,6) were used to examine the sensitivity of pit retention of dust to the wind speed. In all the cases, northerly winds and neutral atmospheric stability was assumed. Further, the emission source was introduced at the pit bottom (Coordinates: X = 3000 ft, Y = 2000 ft, based on True North) at the release height of 7 feet. The aerodynamic particle size introduced in all these cases was 10 μ. In order to examine the effect of

only the wind speed, it was essential to hold all other parameters constant.

Results: The patterns of winds in all the test cases, i.e. with wind speeds of 2 miles/hr, 6 miles/hr, 10 miles/hr, and 30 miles/hr were found to be similar. Figure 4.3 and 4.4 illustrate the wind patterns for Case 1. Figure 4.3 shows the wind flow pattern at a vertical section taken at X = 3000 feet, while Figure 4.4 shows the wind flow pattern at a horizontal section taken at Z = 6290 feet. It was observed that wind is affected by the terrain features. In particular, it was seen that wind changed directions while it moved in the Bingham Canyon.

The dust trajectories generated for the four cases are presented as Figures 4.5 through 4.8. In general, as the wind speed increases, the dispersion pattern spreads more horizontally and vertically. This can be attributed to increased turbulent kinetic energies, as wind speed increases. Figure 4.9 illustrates the trajectories for case 1 (wind speed 6 miles/hr) viewing along the X-direction. As mentioned earlier, the escape fraction can be estimated as the fraction of escaping particle trajectories out of the total 500 trajectories introduced at the emission point. The escape fractions were found to be 10.2%, 11.8%, 12.4%, and 12.6% for test cases 4, 1, 5, and 6, respectively. Thus, it can be concluded that as wind speed increases, a higher fraction of particles will leave the boundaries of the pit. The result is also

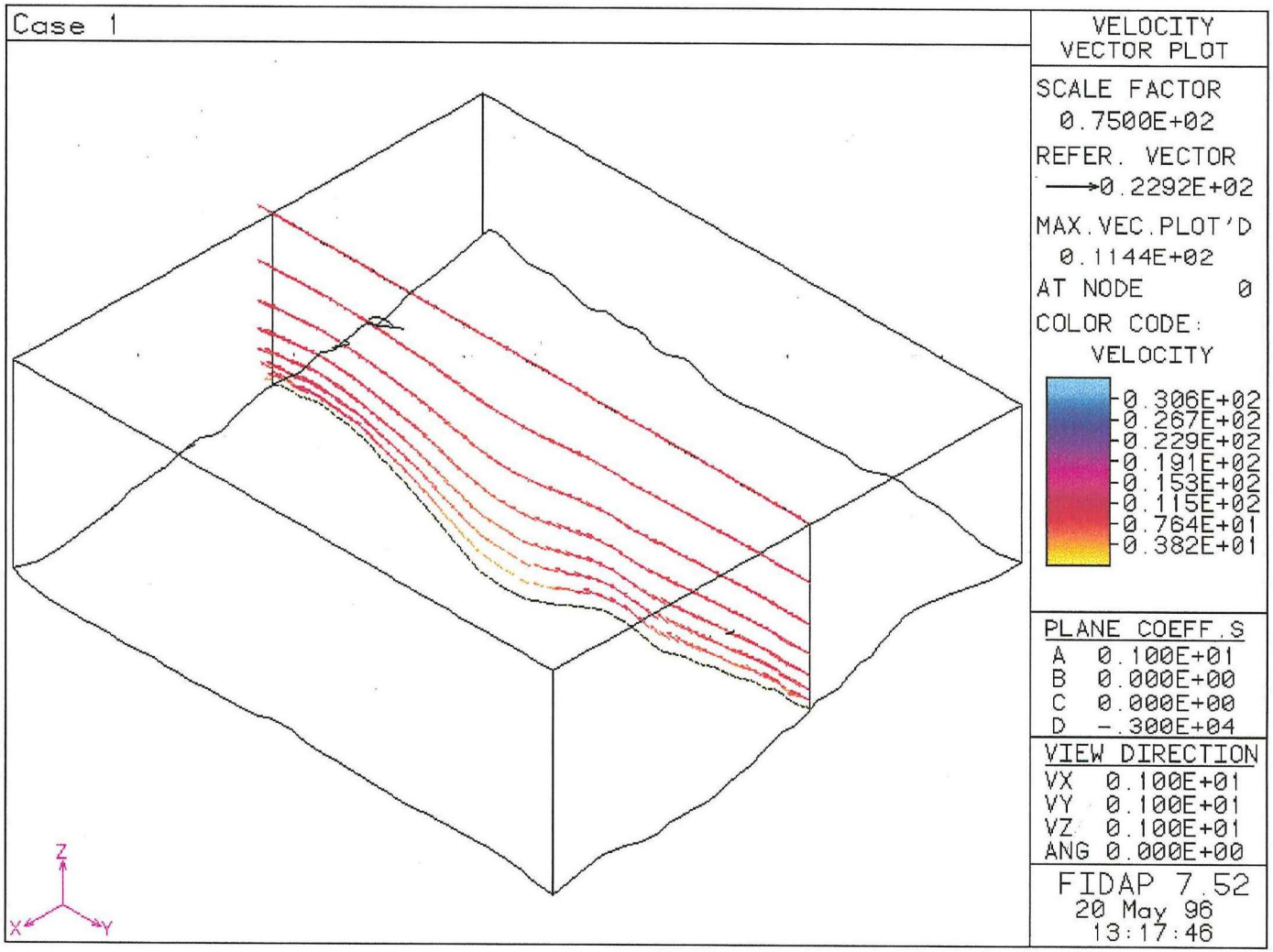

Figure 4.3 Wind flow patterns for case 1
(at section TE (or X)=3000 feet)

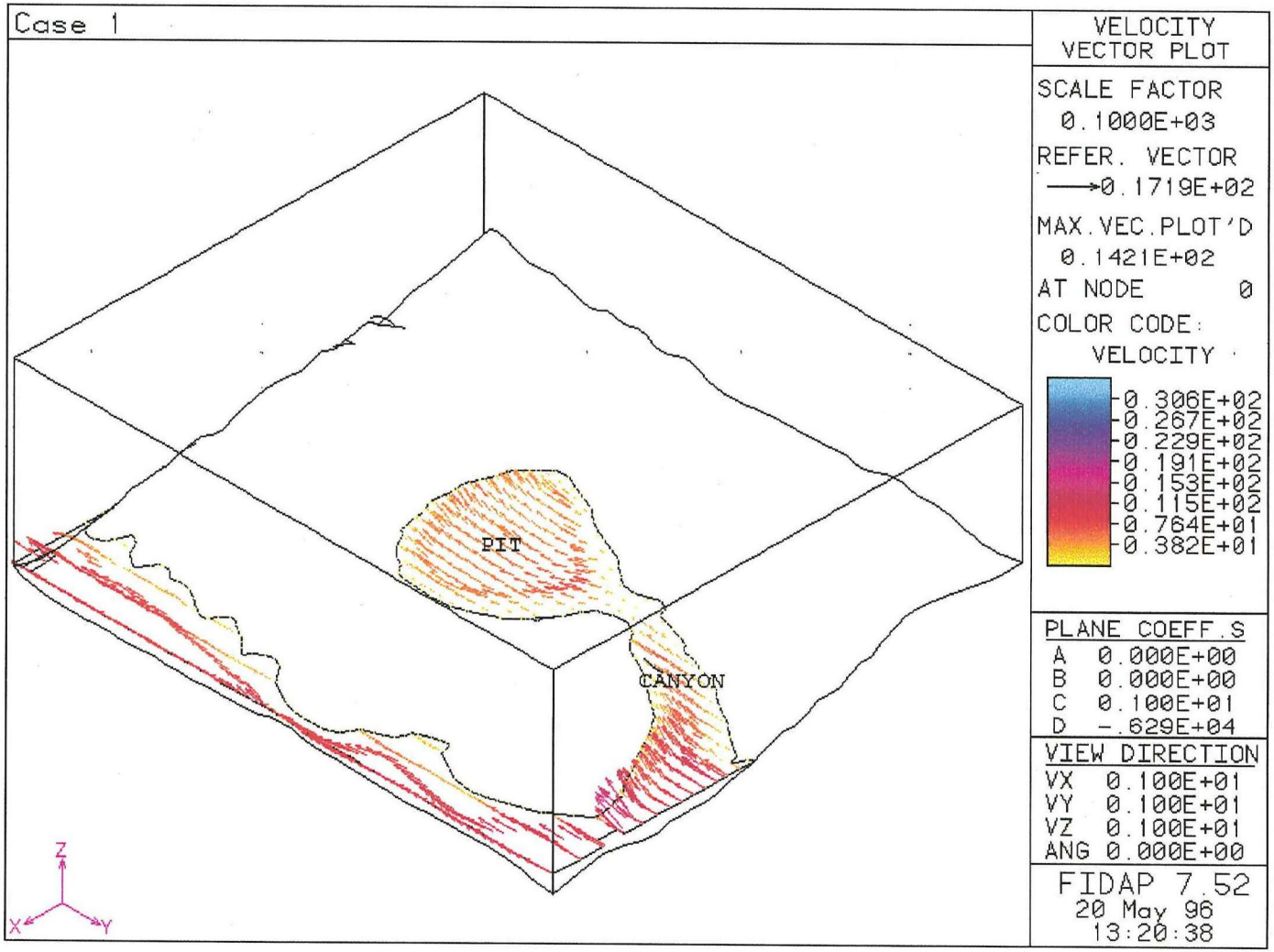

Figure 4.4 Wind flow patterns for case 1
(at section Z=6290 feet)

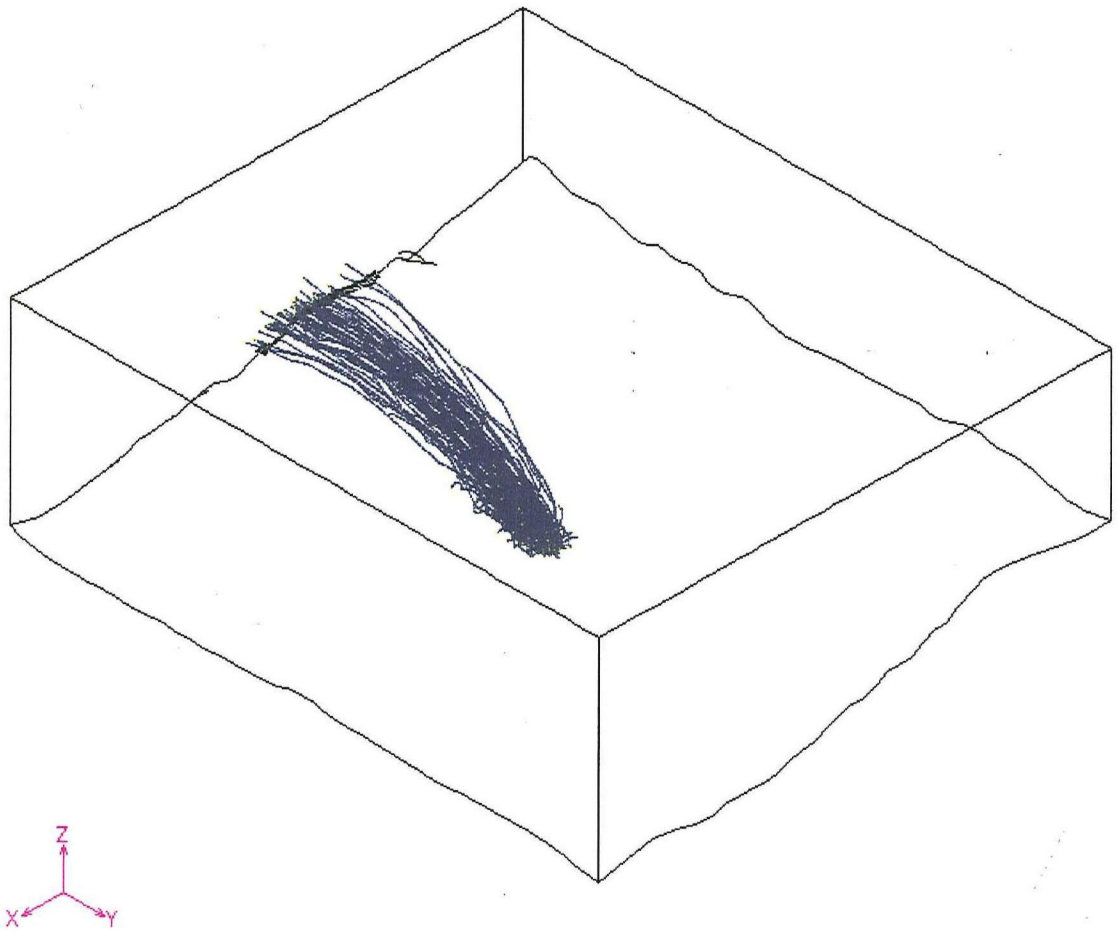

Figure 4.5 Particle trajectories for case 4
(wind speed 2 miles/hour)

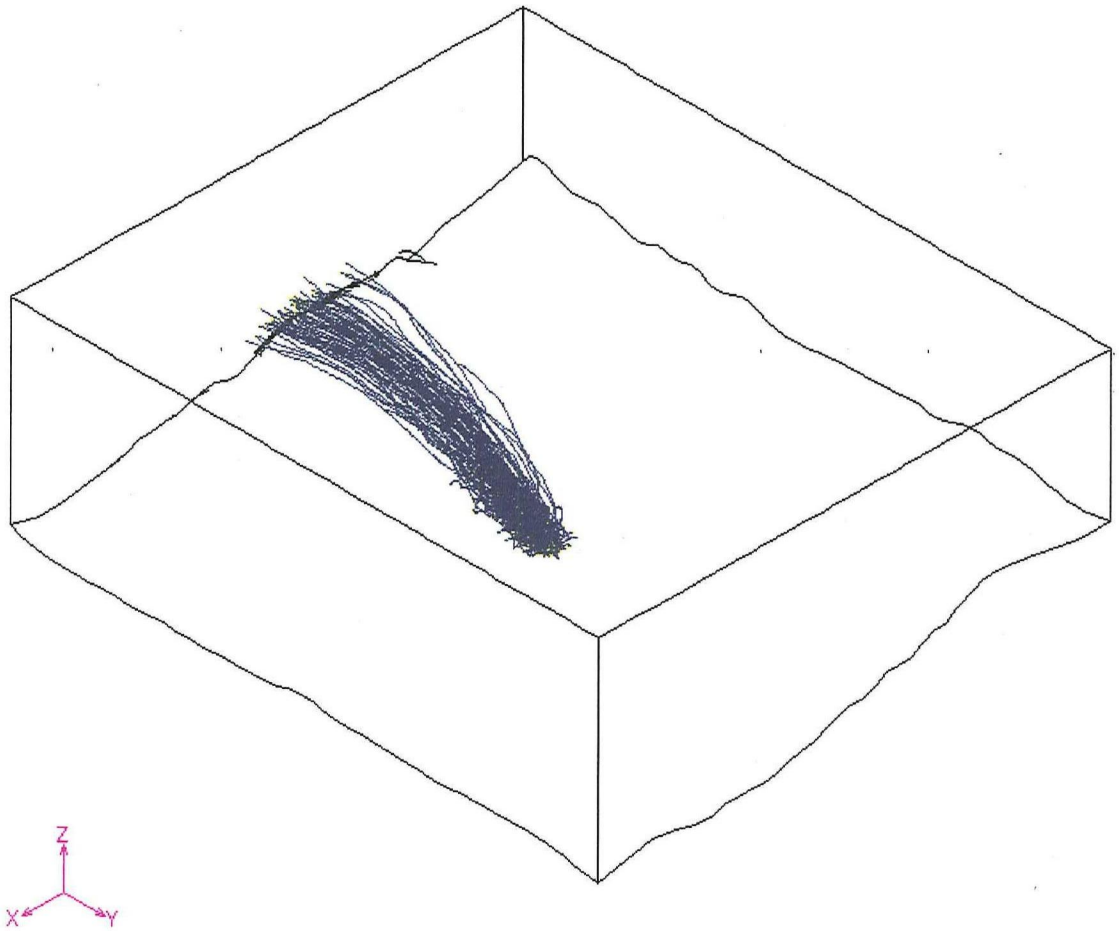

Figure 4.6 Particle trajectories for case 1
(wind speed 6 miles/hour)

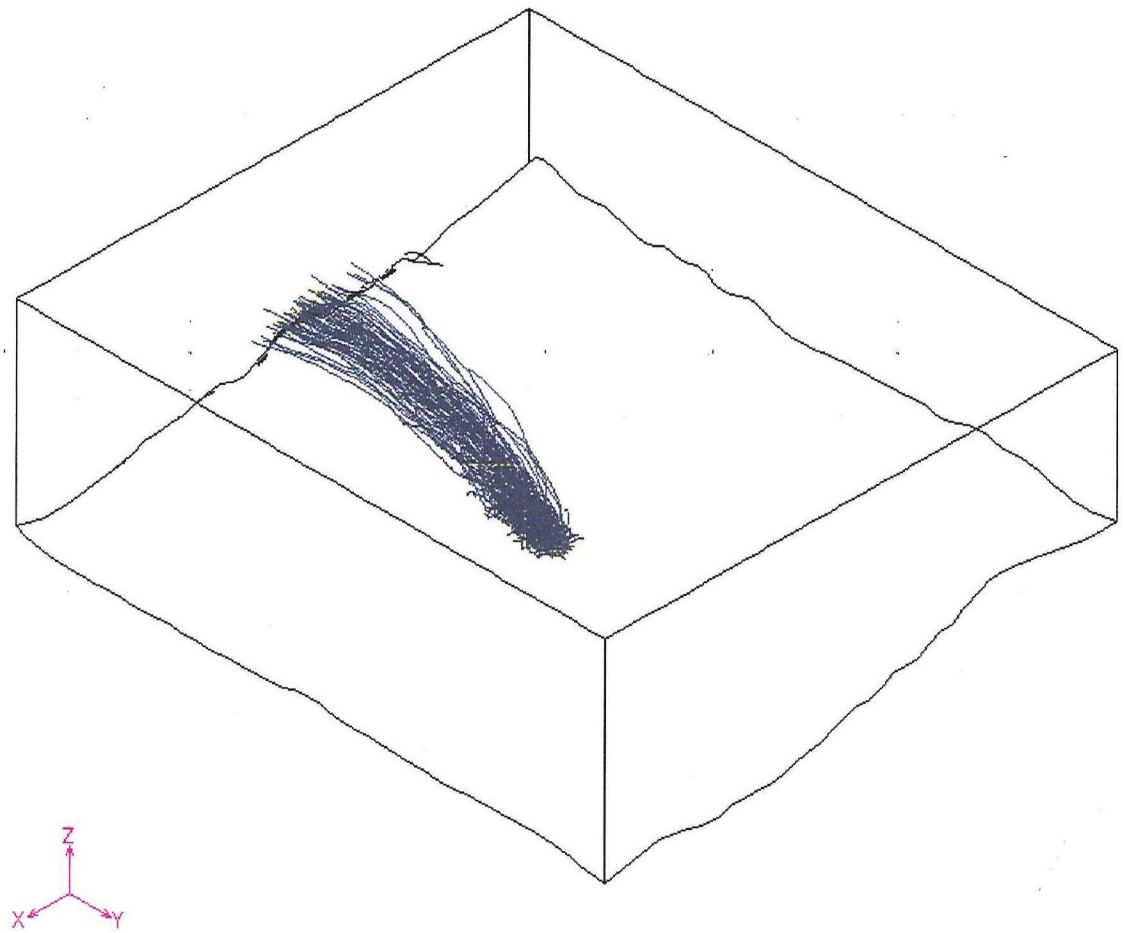

Figure 4.7 Particle trajectories for case 5
(wind speed 10 miles/hour)

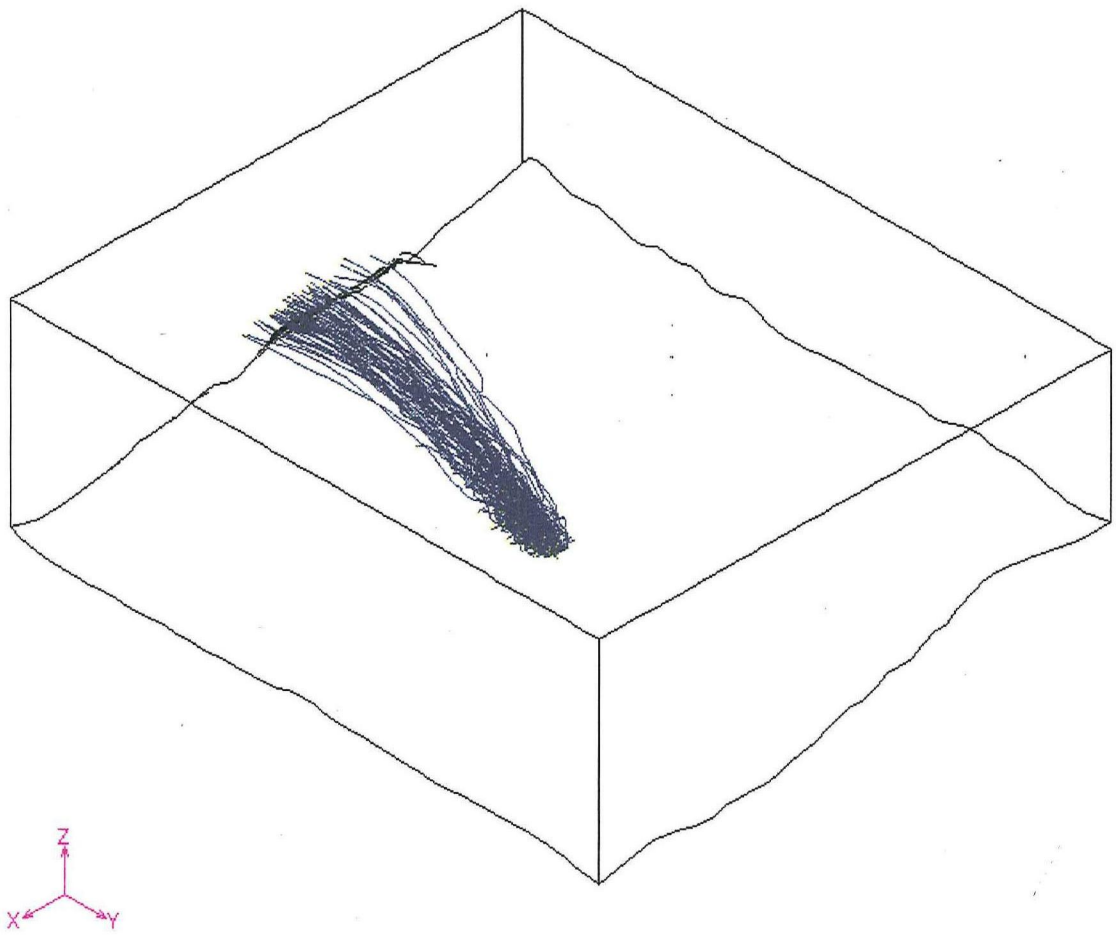

Figure 4.8 Particle trajectories for case 6
(wind speed 30 miles/hour)

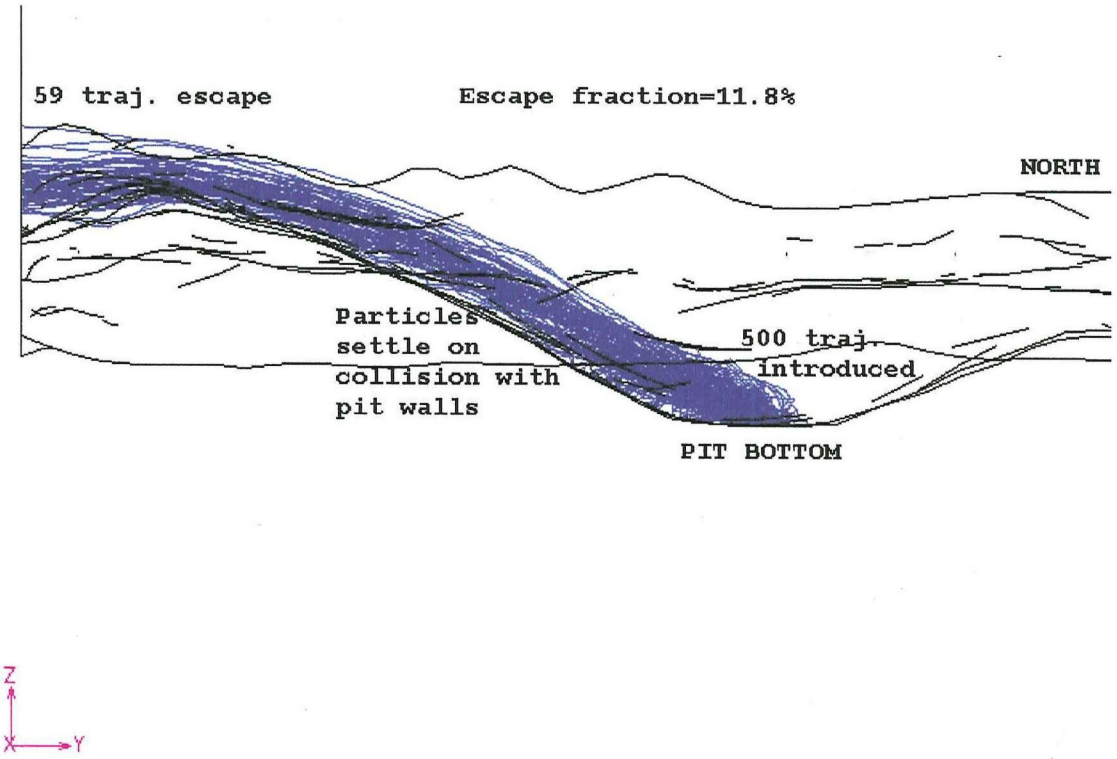

Figure 4.9 Particle trajectories for case 1 (wind speed 6 miles/hour), view along X-direction

illustrated in Figure 4.10. It seems that at higher speeds, the increase of escape fraction with wind speed becomes less pronounced.

4.3.2 Sensitivity to Wind Direction

Four cases (1,7,8,9) were used to examine the sensitivity of pit retention to the wind direction. In all cases, a wind speed of 6 miles/hr and neutral stability was assumed. The emissions were introduced at pit bottom at the coordinates X = 3000 feet, Y = 2000 feet at a release height of 7 feet, and the aerodynamic particle size of 10 μ.

Results: The results for Case 1 with a pit bottom source at a release height of 7 feet have already been discussed. The results for cases 7,8 and 9 were additionally evaluated.

After analysis of the particle trajectories, the escape fractions were computed to be 11.8%, 12.6%, 12.2%, and 12.4% for the northerly, southerly, westerly, and easterly winds, respectively. Since the emission point is not equidistant from the respective downstream boundaries, the pit retention/escape fraction cannot be compared based on the wind direction. However, one conclusion that can be drawn is that in the case of southerly winds (Case 7), the particles which escape from the pit somewhat follow the contours of the Bingham Canyon. This effect is shown by Figure 4.11 and Figure 4.12. Figure 4.11 is a velocity

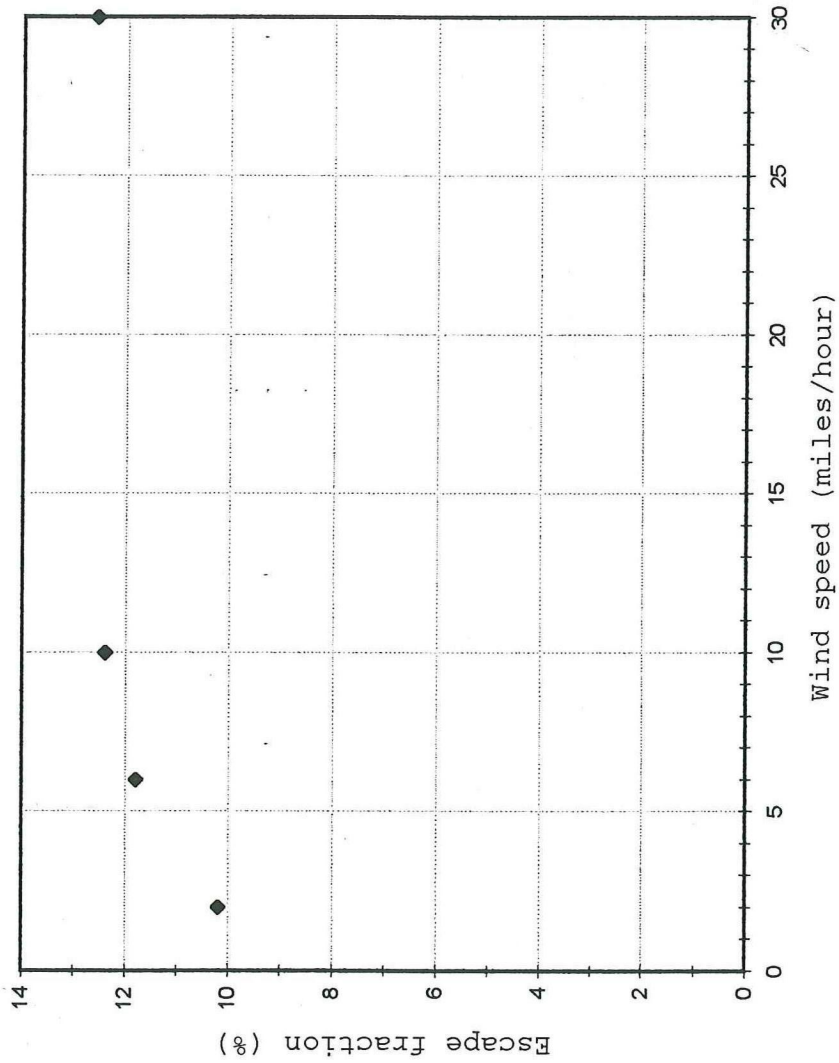

Figure 4.10 Sensitivity of escape fraction to wind speed

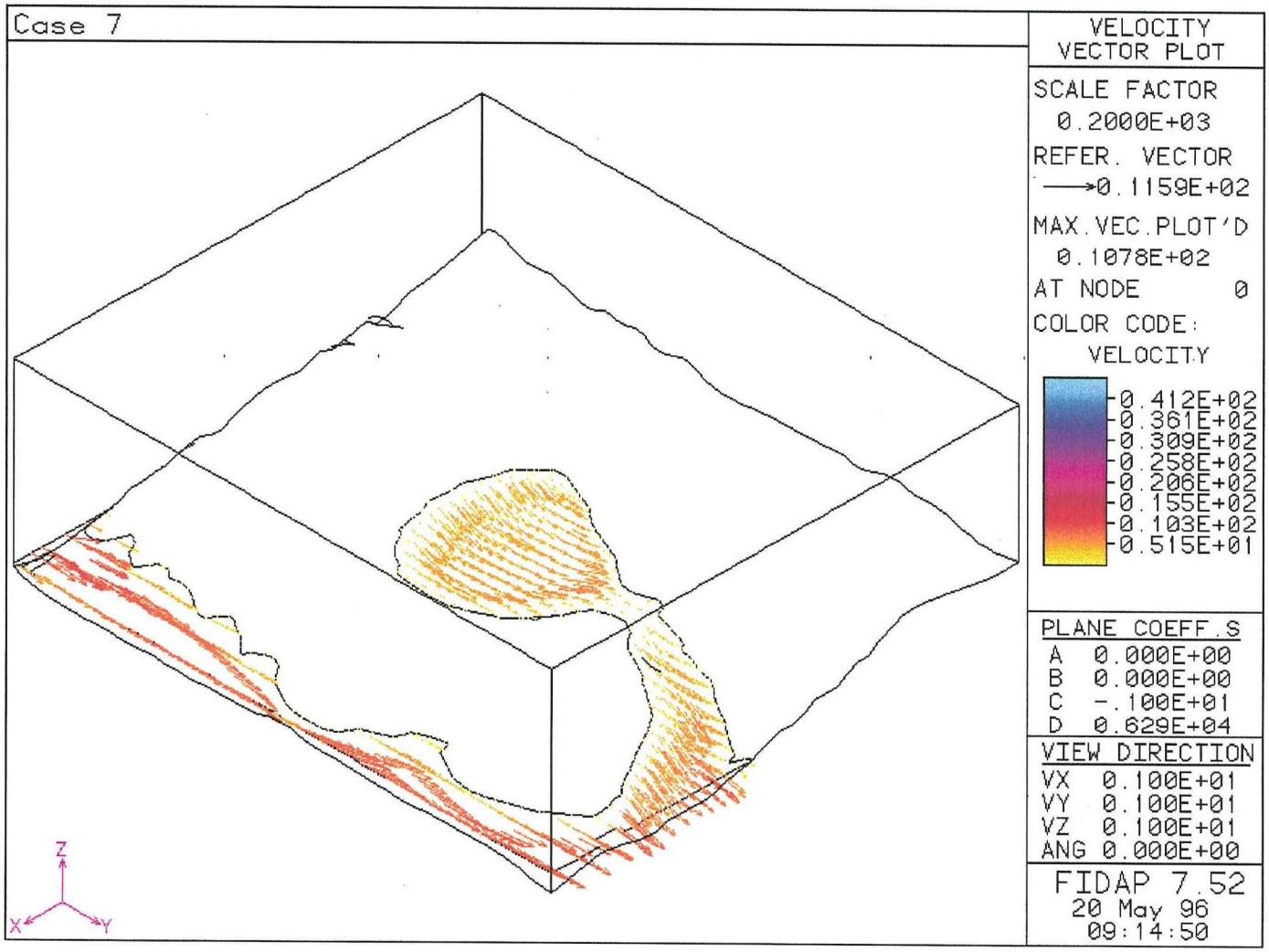

Figure 4.11 Velocity vector plot for southerly winds at Z=6290 feet

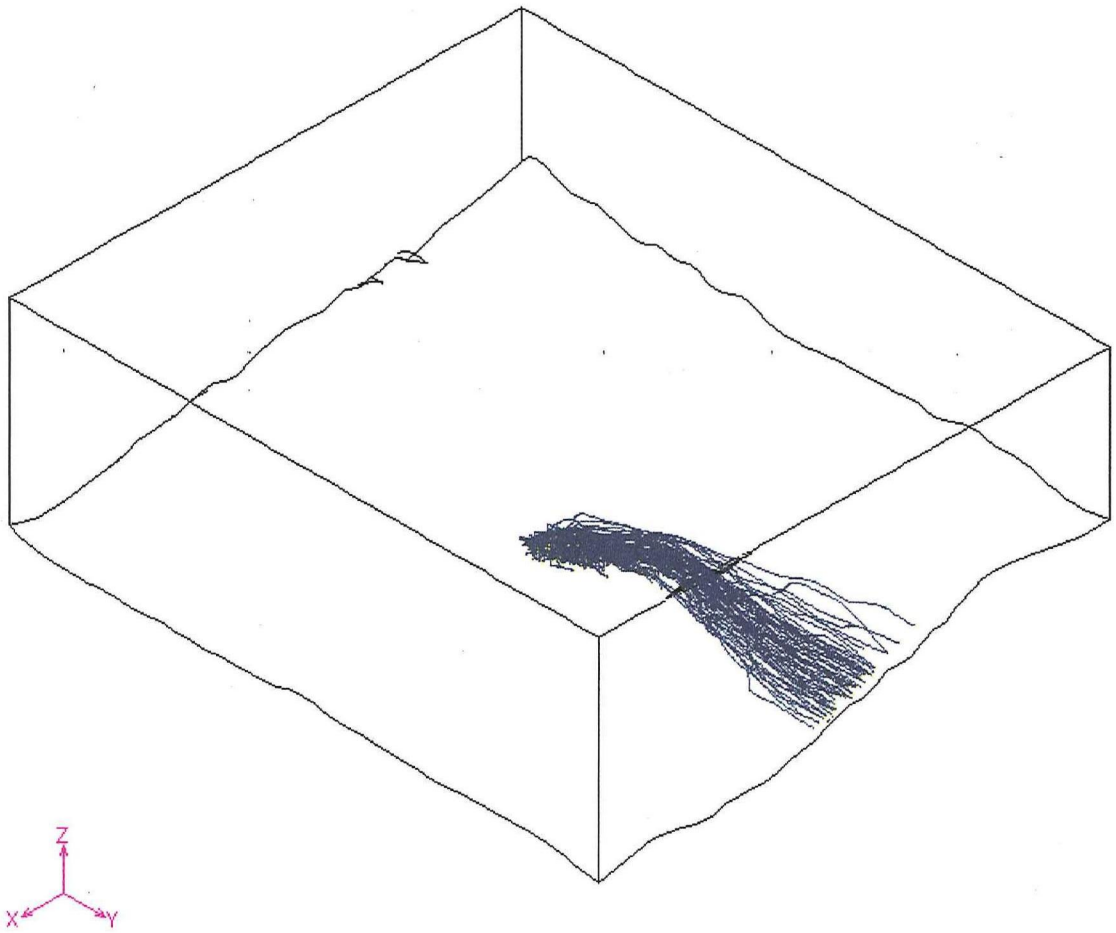

Figure 4.12 Particle trajectories for southerly winds

vector plot at the horizontal section taken at Z = 6290 feet, and Figure 4.12 is the corresponding particle trajectory plot. Hence, a slightly higher escape fraction (12.6%) was obtained for southerly winds in spite of the greater distance of travel to the downstream boundary.

4.3.3 Sensitivity to Atmospheric Stability

Three cases (2,1,3) which represent stabilities A, D and F, respectively, were used to examine the sensitivity to atmospheric stability. In all the cases, northerly winds with speeds of 6 miles/hour were assumed. Again, the emission point was located at X = 3000 feet, Y = 2000 feet at a release height of 7 feet above ground, and was releasing 10 μ particles.

Results: The particle trajectories obtained for the three situations are shown by Figures 4.13, 4.6 and 4.14. As anticipated, the spread in the horizontal and vertical directions was found to be maximum for unstable conditions (Case 2), minimum for stable conditions (Case 3) and intermediate for neutral conditions (Case 1). This is because as the air becomes more unstable, the higher magnitude of wind fluctuations and eddy sizes cause more dispersion/spread of the trajectories. Quantitatively, the escape fractions were found to be 12.6%, 11.8% and 12.2% for unstable, neutral and stable conditions, respectively.

If a relationship such as Winges equation (Equation

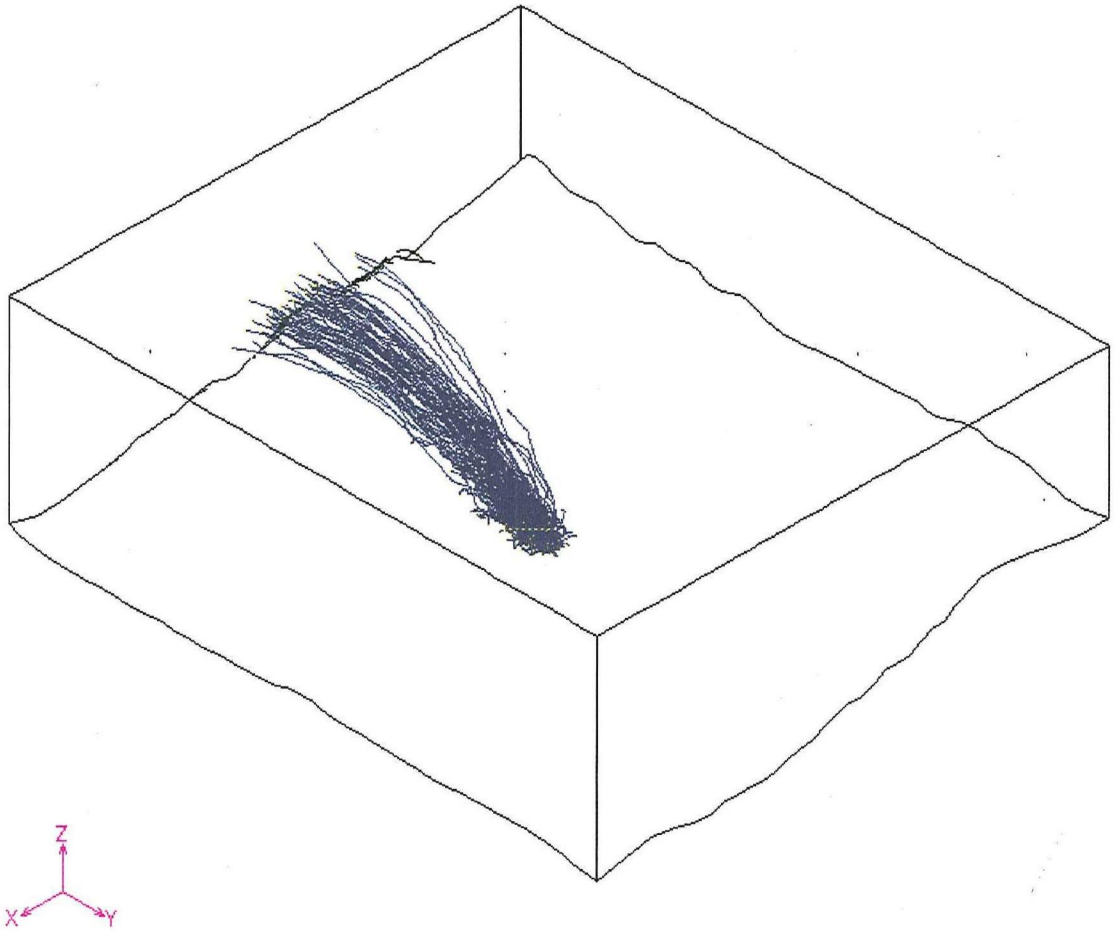

Figure 4.13 Particle trajectories for unstable (case 2) conditions

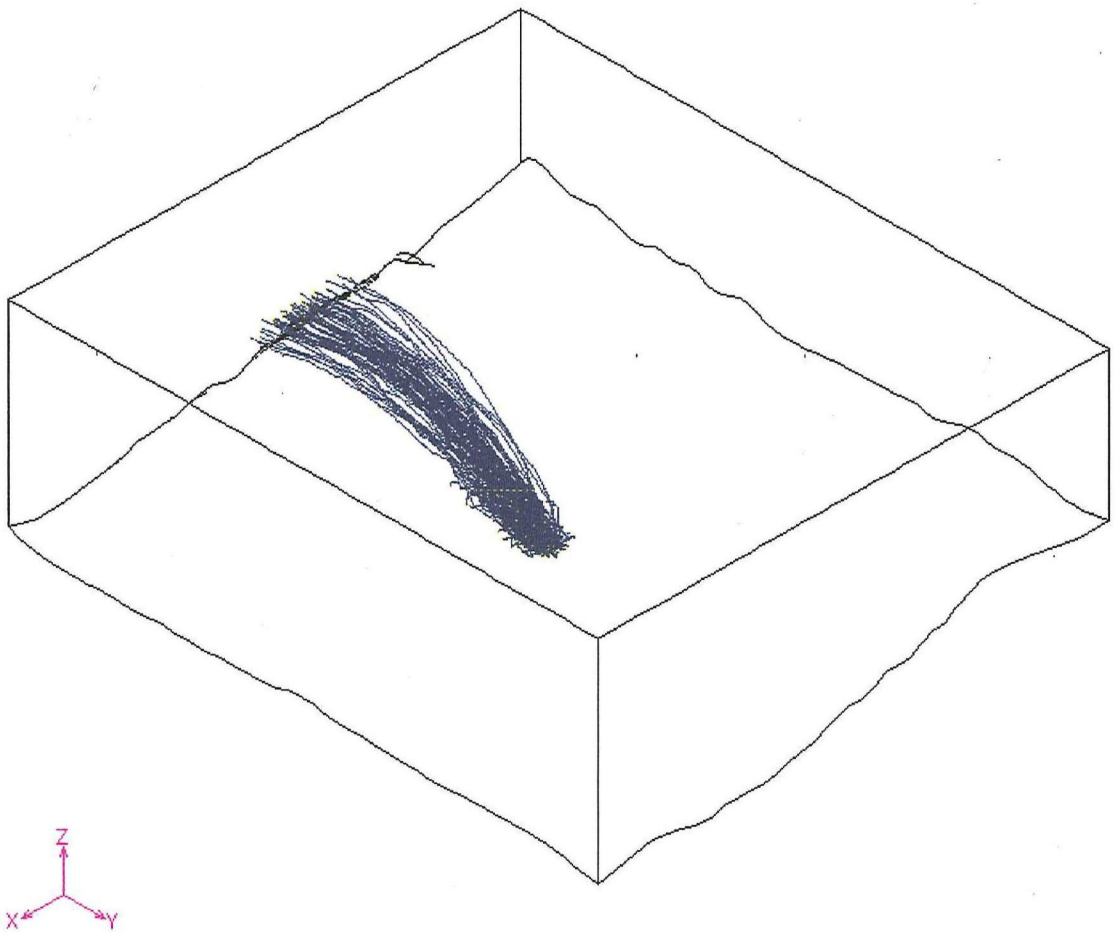

Figure 4.14 Particle trajectories for stable (case 3) conditions

(1.2)) was being used to estimate the escape fraction, one would conclude that the escape fraction should be maximum for unstable conditions and should decrease as the atmosphere becomes more stable. However, as mentioned earlier, Winges equation treats a very simplified dispersion scenario. One of the limiting assumptions of the Winges equation is that turbulent diffusion is the only mechanism for the transport of material out of the pit, and the convection due to the wind is ignored.

Realistically speaking, the convection by wind is probably a very important phenomenon which causes transfer of the material downwind. Hence, it is possible that under stable conditions (where the spread of trajectories is minimum), fewer particles might get trapped due to the interaction with the pit walls and a higher fraction could be transported downwind. This explains the probable cause of the higher value of escape fraction obtained for stable conditions (12.2%) in the Bingham pit study.

4.3.4 Sensitivity to Source Location and Height

4.3.4.1 Source location. Case 1 was used to analyze the sensitivity of the pit retention/escape fraction to source location. In Case 1, northerly wind with a speed of 6 miles/hr and neutral stability was used. Particles with an aerodynamic diameter of 10 μ were introduced at three locations in the pit. For all three locations, the release height of 7 feet above the ground

was used. The three locations evaluated were:

- pit bottom (X = 3000 feet, Y = 2000 feet)
- a source near the downwind boundary of the domain (X = 3000 feet, Y = -3000 feet), which represents the so-called "worst" case scenario
- a source near the in-pit crusher (X = 4190 feet, Y = 3220 feet), chosen as this is a high-activity area.

Results: Under the conditions of the simulations, the escape fractions were found to be 11.8%, 19.2% and 16.6% for the three locations (in the same order mentioned earlier). These escape fractions follow the expected trend: the deeper the source in the pit, the lesser the escape fraction. The particle trajectories for the source near the downwind boundary and for the source near the in-pit crusher is illustrated by Figures 4.15 and 4.16.

4.3.4.2 Source height. Case 1 was used to analyze the sensitivity to source height. Particles with an aerodynamic size of 10 μ were introduced at the pit bottom (X = 3000 feet, Y = 2000 feet) in both cases. Two source heights were considered in the evaluation: 7 feet (to represent sources such as haul roads) and 30 feet (to represent sources such as truck loading by a shovel).

Results: As explained earlier, the escape fraction for the 7 feet high source was calculated to be 11.8%. For the release height of 30 feet, the escape fraction was

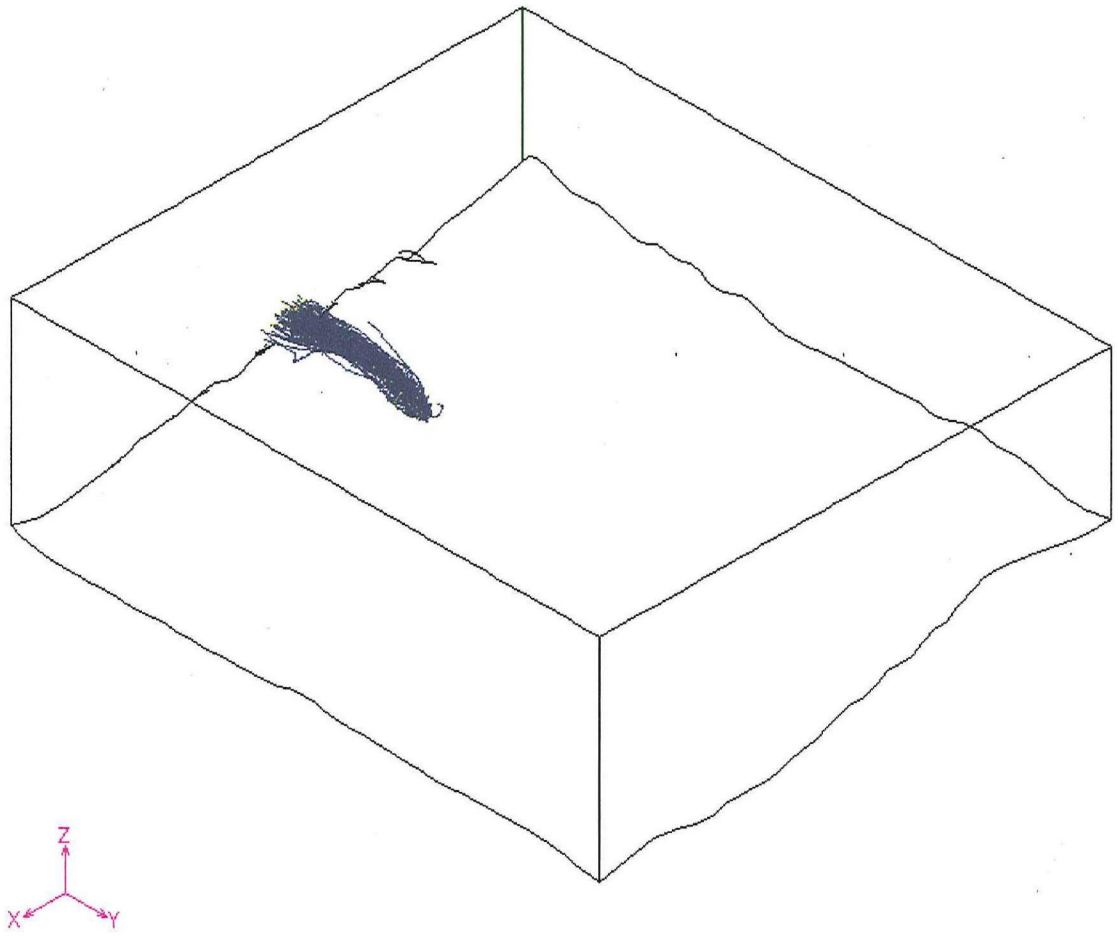

Figure 4.15 Particle trajectories for near-downwind boundary emission source ("worst-case scenario")

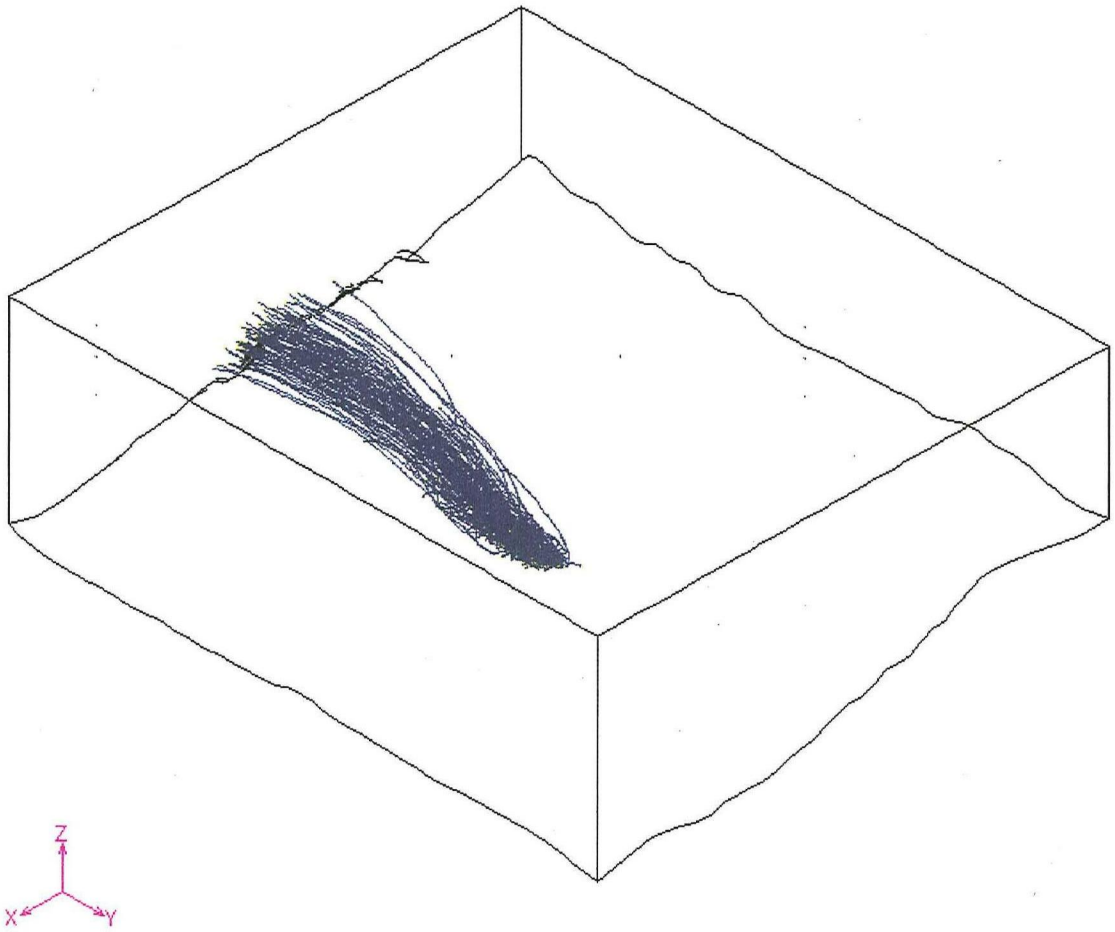

Figure 4.16 Particle trajectories for near-in-pit crusher emission source

found to be 13.4%. A higher value of escape fraction was obtained for the 30 feet high source as it encounters higher wind speeds and thus, the probability for the trajectories to cross the downstream domain becomes greater.

4.3.5 Sensitivity to Particle Sizes

Case 1 was again used to study the sensitivity of the escape fraction to particle sizes. In all the cases, the source location used was the pit bottom (X = 3000 feet, Y = 2000 feet) at the release height of 7 feet.

It should be clarified that the particle sizes used here are aerodynamic particle sizes (with unit density). This was done as EPA's standards for air quality exist for PM-10, and PM-10 refers to particles with aerodynamic diameters smaller than 10 μ.

Results: Several aerodynamic particle sizes (1 μ, 2 μ, 5 μ, 7 μ, 10 μ, 15 μ, 20 μ, 30 μ, 50 μ and 80 μ) were introduced at the emission point. The results are shown in Figure 4.17. As the particle size was increased, the escape fraction decreased. This is due to increased values of terminal settling velocities (and hence more gravitational settling) for larger particles. The escape fraction for PM-10 in this case is approximately 12.4%.

Figure 4.18 illustrates comparison of the results obtained with the different escape fraction equations. The mathematical expressions for all these equations have

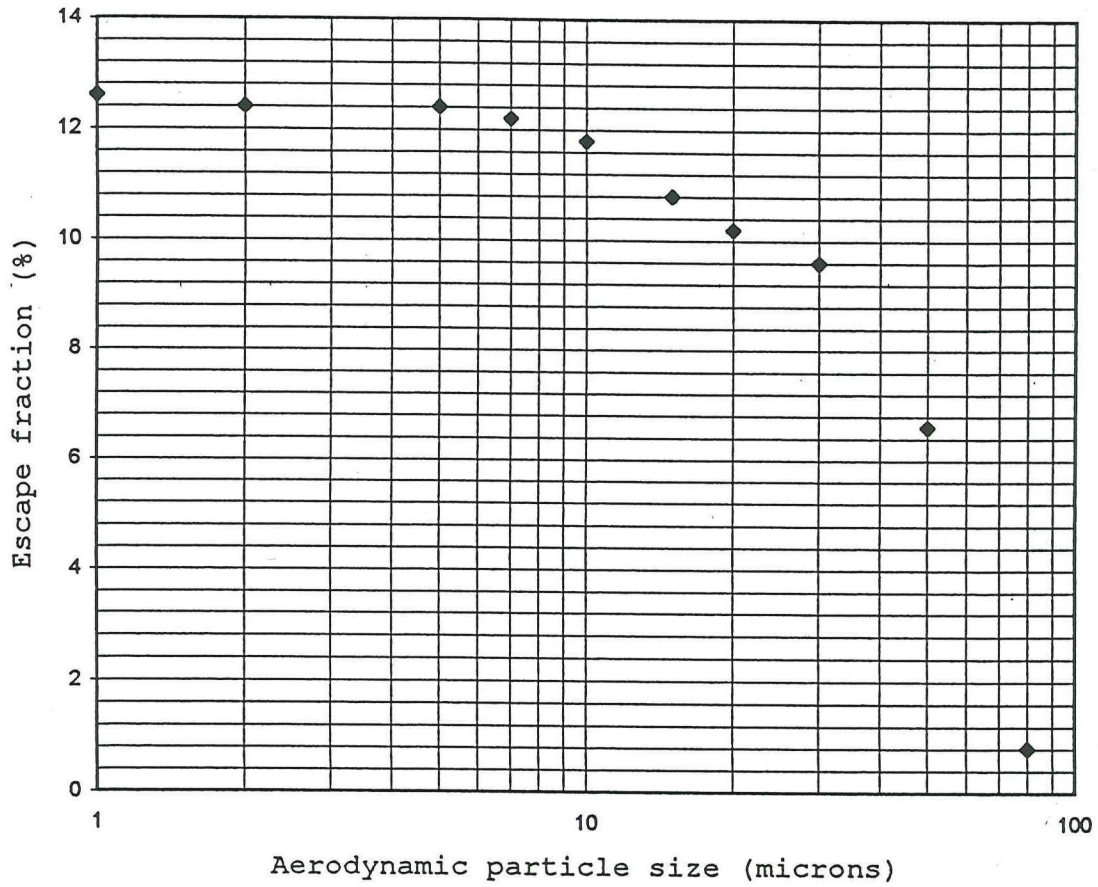

Figure 4.17 Sensitivity of escape fraction to aerodynamic particle size

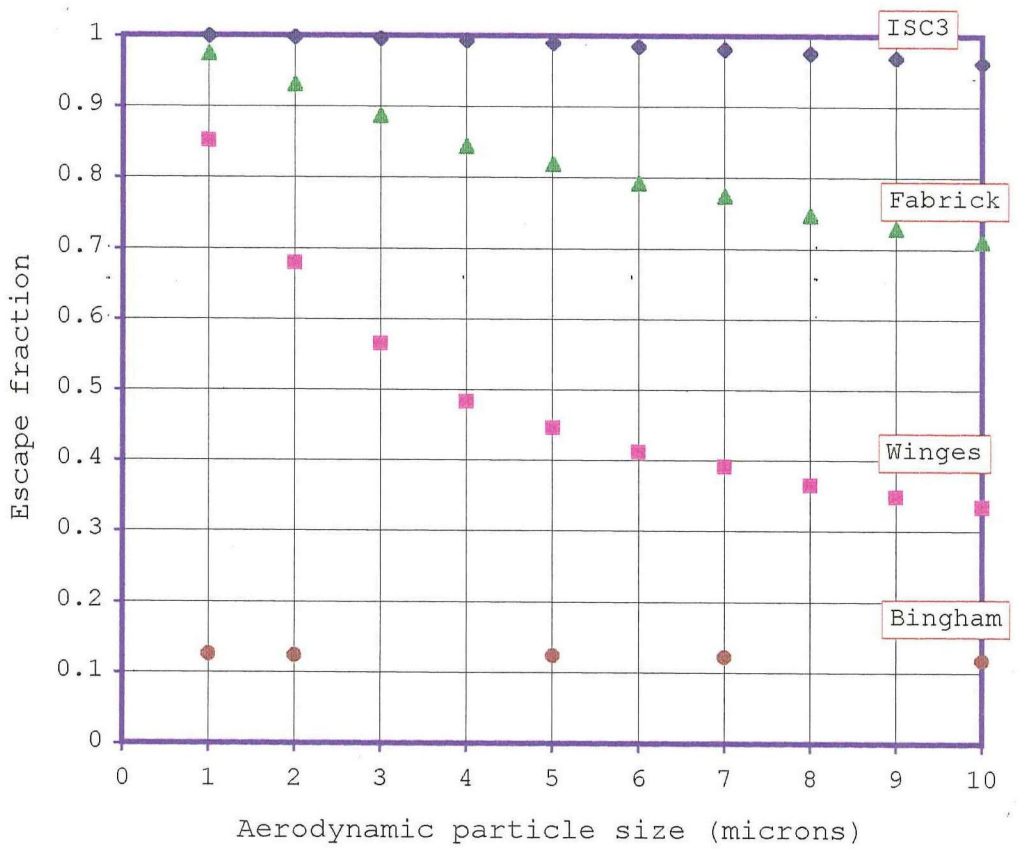

Figure 4.18 Comparison with different escape fraction equations

been explained in Chapter 1. Due to the simplified nature of these equations, certain assumptions were necessary to apply these for the Bingham pit. For instance, H was specified as 2750 feet (838.4 m), and K_z was specified as 6.74 m^2/sec (same as eddy viscosity computed for neutral, 6 miles/hour conditions) in the Winges model. The width of the pit was specified as 8150 feet (2484.7 m) in the Fabrick's equation. The value of deposition velocities for different particle sizes were computed using Figure 10.4 of Hanna, et al., 1982, using z_o=10 cm and density of particles as 1 gm/cm^3. The size dependent escape fractions were then computed. As shown by Figure 4.18, it can be concluded that the model predicts values of escape fraction much lower than the values that are computed using simple escape fraction equations. This observation highlights existence of unique conditions regarding pit retention for the Bingham Canyon mine. Due to the large size of the pit, much of the emissions that are released tend to remain inside the pit and this leads to low values of escape fraction.

CHAPTER 5

VALIDATION AND COMPARISON

5.1 Numerical Tests and Validation

Numerical models are mathematical tools which use a set of numerical algorithms that describe the physical aspects of the problem. It is therefore essential to conduct numerical tests and validation on the model to develop an understanding of its performance. The performance of the numerical model can be demonstrated by comparing its results with experimental/analytical results for some classical simple problems. If the model predicts the results similar to those obtained with analytical or experimental studies, the model can be applied to more complex situations for which analytical/experimental results do not exist.

The analysis of airflow patterns and pit retention of dust for the Bingham Canyon mine involved simulation of flow fields and particle trajectories. For the simulation of turbulent flow, the standard κ-ϵ model (along with near wall modeling) was used. The particle behavior was predicted with the Lagrangian formulation.

Although FIDAP is a commercial software whose validity has been checked over the years, it was still

considered important to perform numerical tests for particular aspects of the Bingham model. Mainly, two validation studies were conducted to test the performance of the flow and particle models.

5.1.1 Turbulent Flow

In the FIDAP Examples manual, there are several cases where the validation of the numerical algorithms have been conducted. For the present study, example 18 of the FIDAP Examples manual, which involves 2-dimensional, steady, turbulent, incompressible flow over a backward-facing step, was used as a basis for the analysis. The values of the different parameters specified are identical to those specified in the manual.

The region of interest consists of a single backward-facing step in a channel. The walls are smooth and impermeable. The geometry of the flow situation, along with the mesh that was generated, is illustrated in Figure 5.1. The height of the step and the channel are one and three, respectively. A constant inflow velocity of one was imposed at the inflow which is located six step heights upstream. The assumption was that fully developed flow is attained before the flow reaches the step. Values for turbulent kinetic energy and dissipation were also specified at the inflow. The outflow boundary was located 24 step heights downstream. A no-slip boundary condition was applied for the wall. The standard

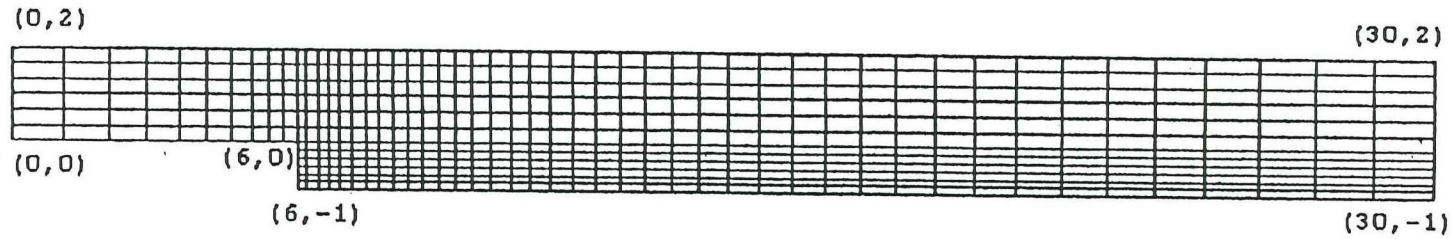

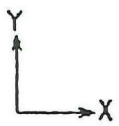

Figure 5.1 Geometry and mesh for the backward-facing step problem

κ-ϵ model with the near wall modeling approach was used for the validation study. The Reynolds number for the simulation was chosen to be 45,000 so as to allow comparison with the experimental data of Kim (1978) (as cited in the FIDAP Examples manual).

The results of the simulation are illustrated in Figure 5.2, which shows the different streamlines. The experimentally observed length of the recirculation region, X_R, was found to be (7.0 $\pm$ 0.5) times the step height (Kim, 1978, as cited in the FIDAP Examples manual). The reattachment length from the FIDAP simulation was 6.43. Although there is a slight underprediction, it is still reasonable to say that the κ-ϵ model performs quite well for the simulation of turbulent flows.

5.1.2 Lagrangian Particle Formulation

The Lagrangian particle formulation of FIDAP was validated using a simple 2-dimensional laminar flow problem. The flow domain was a rectangular area 3 m (along the flow) by 2 m (crossflow vertical direction). The rectangular mapped mesh generated for the domain is illustrated in Figure 5.3. A constant velocity of 1×10^{-2} m/s was assigned to the inflow boundary. The alongwind boundaries of the domain were specified as symmetry boundaries, which means that the vertical component of velocity was specified to be zero. Air viscosity and density were specified as 1.8×10^{-5} Pa-sec

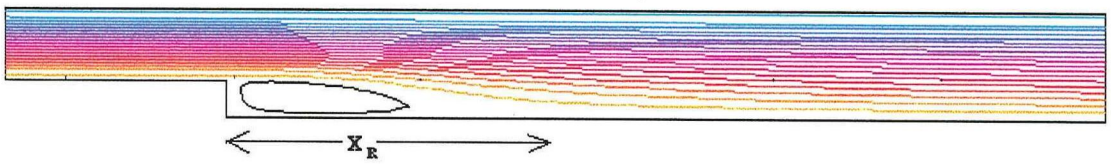

Figure 5.2 Streamlines for the backward-facing step problem

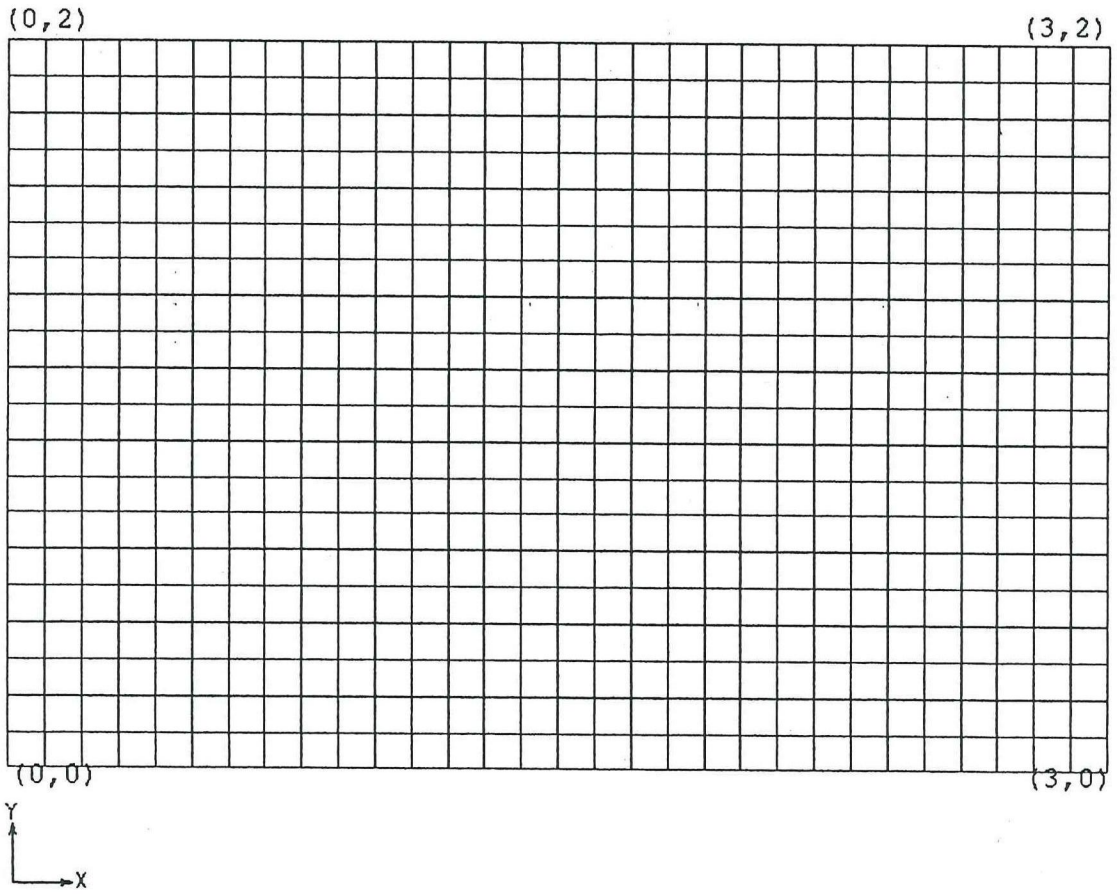

Figure 5.3 Rectangular mapped mesh for the particle formulation validation problem

and 1.2 kg/m^3, respectively. Based on the data mentioned, FIDAP was used to calculate the flow field in the domain.

After the laminar flow problem was solved, a single 10 μ particle of density 2000 kg/m^3 was introduced in the domain at the coordinate (X = 1, Y = 1). The acceleration due to gravity was specified as 9.81 m/sec^2. The trajectory of the particle was tracked with 0.01 second increments for 100 seconds. The computed flow field and the particle trajectory is illustrated in Figure 5.4. In 100 sec, the particle was carried about 0.995 m along the flow and about 0.604 m vertically downwards. Only Stokes drag and gravity forces were considered in this evaluation.

Hand calculations were performed to evaluate the performance of the Lagrangian formulation used in FIDAP. In this case where the flow field is horizontal, Equation (2.35) reduced to the following form for the vertical component of particle velocity

$$\frac{du_{py}}{dt} = \frac{-u_{py}}{\tau} + \left(\frac{\rho_p - \rho_f}{\rho_p}\right) g \qquad (5.1)$$

where u_{py} is the vertical component of particle velocity. All other parameters have been explained earlier. The terminal settling velocity can be obtained by using the relation

$$\frac{du_{py}}{dt} = 0 \qquad (5.2)$$

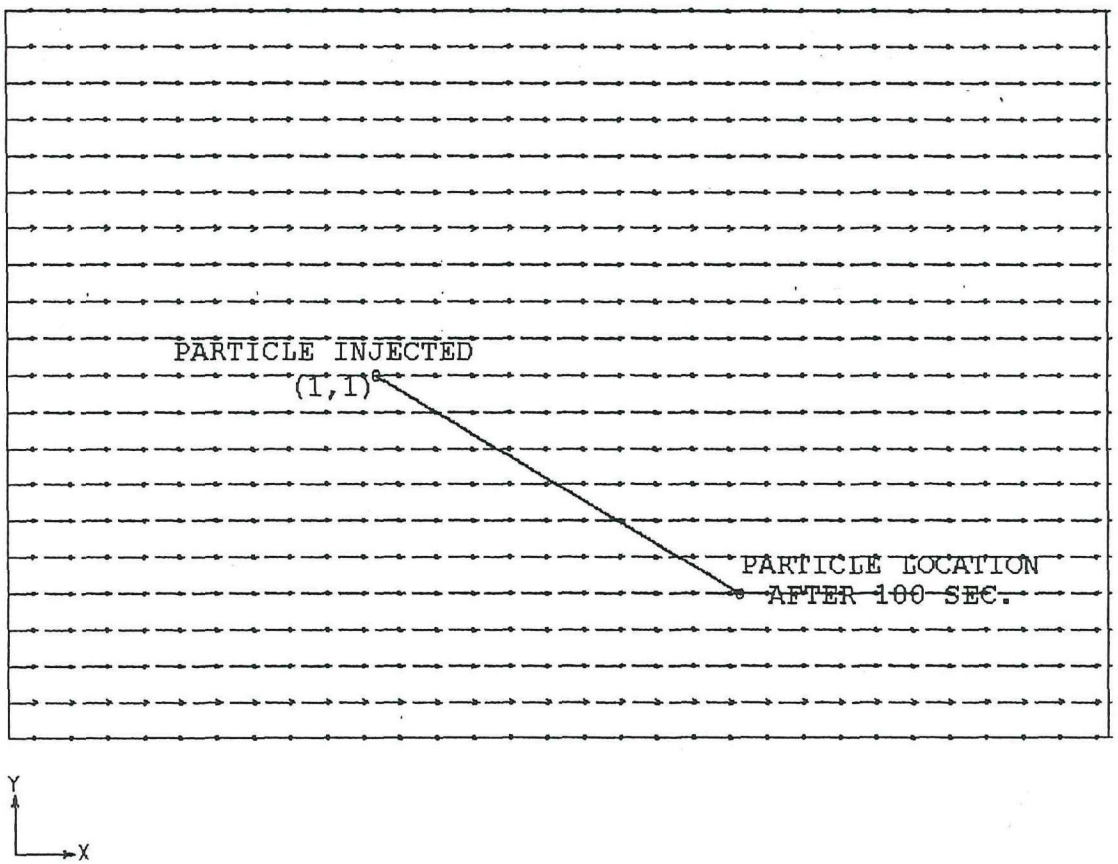

Figure 5.4 Flow field and particle trajectory for the particle formulation validation problem

$$\Rightarrow \quad \frac{-u_{py}}{\tau} + \left(\frac{\rho_p - \rho_f}{\rho_p}\right) g = 0. \qquad (5.3)$$

Using Stokes drag coefficient, $C_D = 24/Re_p$, in the expression for τ (Equation 2.36), Equation 5.3 simplifies to the relation for Stokes terminal settling velocity.

$$u_{py} = \frac{g\, D_p^2\, (\rho_p - \rho_f)}{18\, \mu}. \qquad (5.4)$$

Using the same value of parameters that were used for FIDAP simulation, u_{py} was computed using Equation 5.4 to be 6.052×10^{-3} m/s. Hence, for a total time period of 100 seconds, the particle will travel 0.6052 m vertically downward. Since the uniform flow field (speed 10^{-2} m/s) also transports the particle downwind, the particle travels 1 m in 100 seconds.

Since the hand calculated values closely match the computed values using FIDAP, the objective of validation was satisfied for the Lagrangian formulation.

5.2 Idealized vs. actual geometries for open-pit mines

The EPA's Industrial Source Complex (ISC) models are especially designed to support the agency's regulatory modeling programs. The ISC3 model (September 1995) includes an algorithm for modeling impacts of particulate

emissions from open-pit sources. In the ISC3 models, one of the main assumptions is that pit emissions have a tendency to escape from the upwind side of the pit. This is due to the presence of a recirculatory profile inside the pit. Wind tunnel modeling studies have demonstrated the presence of such a profile. These concepts/studies have been explained in sections 1.1.1.2 and 1.1.3.

In conducting the present study using 3-dimensional finite element modeling for the Bingham Canyon mine, such recirculatory profiles were not observed. This discrepancy led to the investigations presented in this section.

The ISC models allow the open-pit source to be characterized by a rectangular shape with an aspect ratio (length/width) of up to 10 to 1. Different wind tunnel modeling studies (Thompson, R. S., 1994; Perry, S. G., et al., 1994) have also considered idealized rectangular shapes for mine models. The vertical cross-section of the scaled wind tunnel models have a trapezoidal shape if the steps are included. In the case of the Bingham Canyon mine, the actual terrain geometry is much different from an idealized rectangular or trapezoidal shape. In the study presented in this section, three numerical models were developed to study the effect of pit geometries on the airflow patterns. It was decided that 2-dimensional analyses will be sufficient to develop a better understanding of the phenomena involved.

The three vertical cross-sectional 2-dimensional models evaluated were:

- actual Bingham pit geometry at section True-East (or X)= 3000 feet. This is a vertical north-south section that approximately passes through the center of the mine,
- an idealized trapezoidal cross-section, and
- an idealized rectangular cross-section.

In all the cases, the evaluation was conducted for neutral atmospheric conditions and a wind speed of 6 miles/hour. The values of meteorological parameters were kept identical to the 3-dimensional Bingham model for a wind speed of 6 miles/hour and neutral stability. The 2-dimensional finite element mesh was created in all cases. Suitable boundary conditions were then applied. Inlet boundaries had prescribed values for components of velocity (u_x and u_y), turbulent kinetic energy, κ, and dissipation, ϵ. The top boundary (mixing height) was defined as a symmetry boundary, whereas the ground was represented as a wall boundary. The downwind boundary was considered as an outflow boundary. These concepts have been discussed in detail in Chapters 3 and 4 for the 3-dimensional case, and are similarly applied for the 2-dimensional case.

5.2.1 Actual Bingham Geometry

As mentioned earlier, a vertical cross-section at True-East (TE) = 3000 feet with northerly winds was used for this case. This case was intended to serve as the basis for comparison against idealized rectangular and trapezoidal cases. The terrain profile and the 2-dimensional mesh generated for this case is shown in Figure 5.5. Appropriate boundary conditions were then assigned and model definition data and fluid properties were specified. A turbulent flow field was generated as a result for this case. It was observed that a recirculation zone was nonexistent. Thus, the results were similar to those in the 3-dimensional case. These results have been presented as Figure 5.6.

5.2.2 Idealized Trapezoidal Geometry

The model for an idealized trapezoidal section was developed in a similar manner as outlined above for the actual geometry case. The only difference in this case was that an idealized trapezoidal shape was used to represent the Bingham pit. The geometry and finite element mesh is illustrated by Figure 5.7. Figure 5.8 is the vector and streamline plot for this case. Recirculation phenomenon was obtained inside the pit in this case. The wind pattern obtained was almost identical to patterns observed by wind tunnel modeling studies (Figure 7 of Thompson, R. S., 1994; or Figure 2 of Perry,

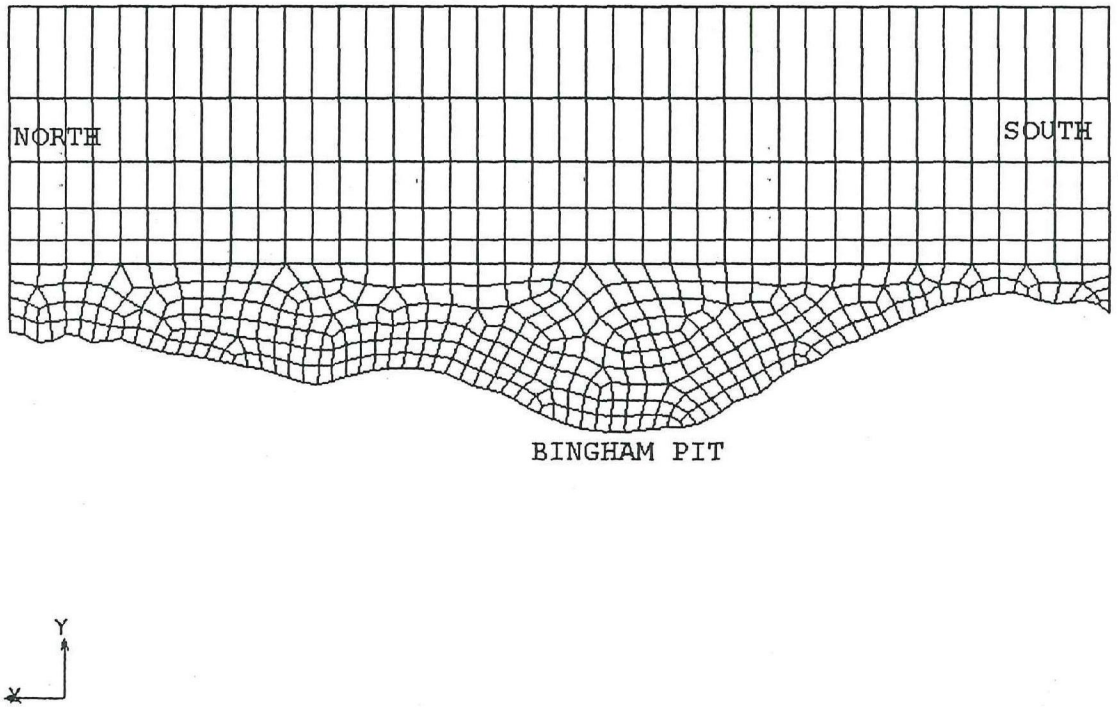

Figure 5.5 Two-dimensional geometry and mesh for the "actual" Bingham case (section at TE=3000 feet)

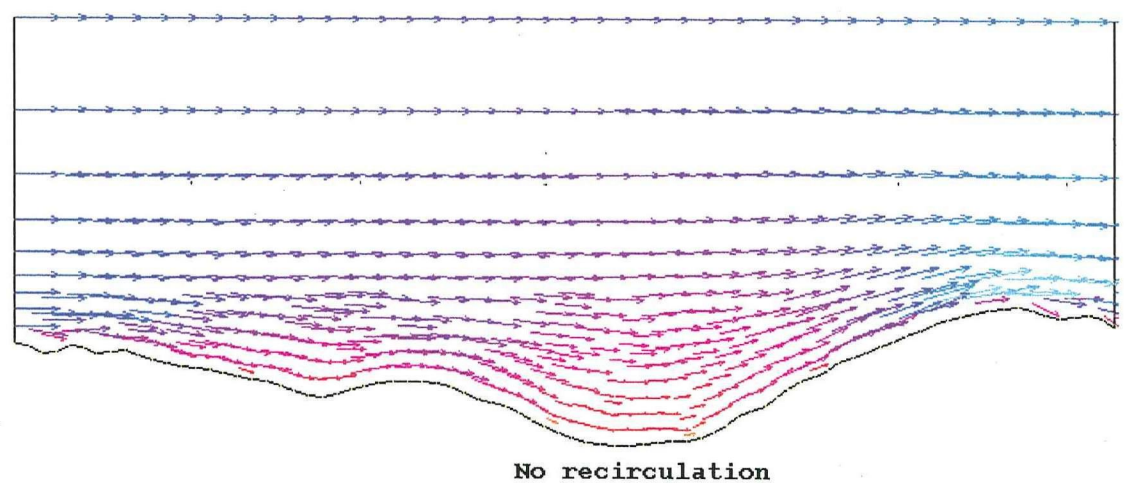

Figure 5.6 Velocity vectors for the "actual" case

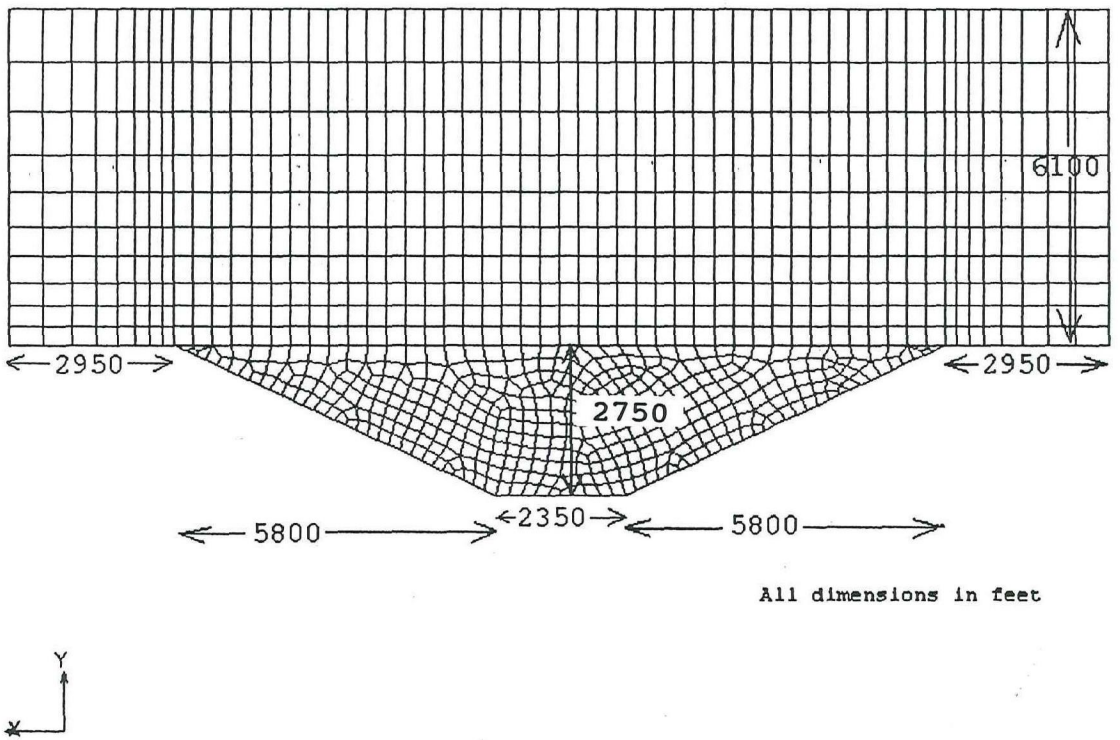

Figure 5.7 Geometry and finite element mesh for the trapezoidal section

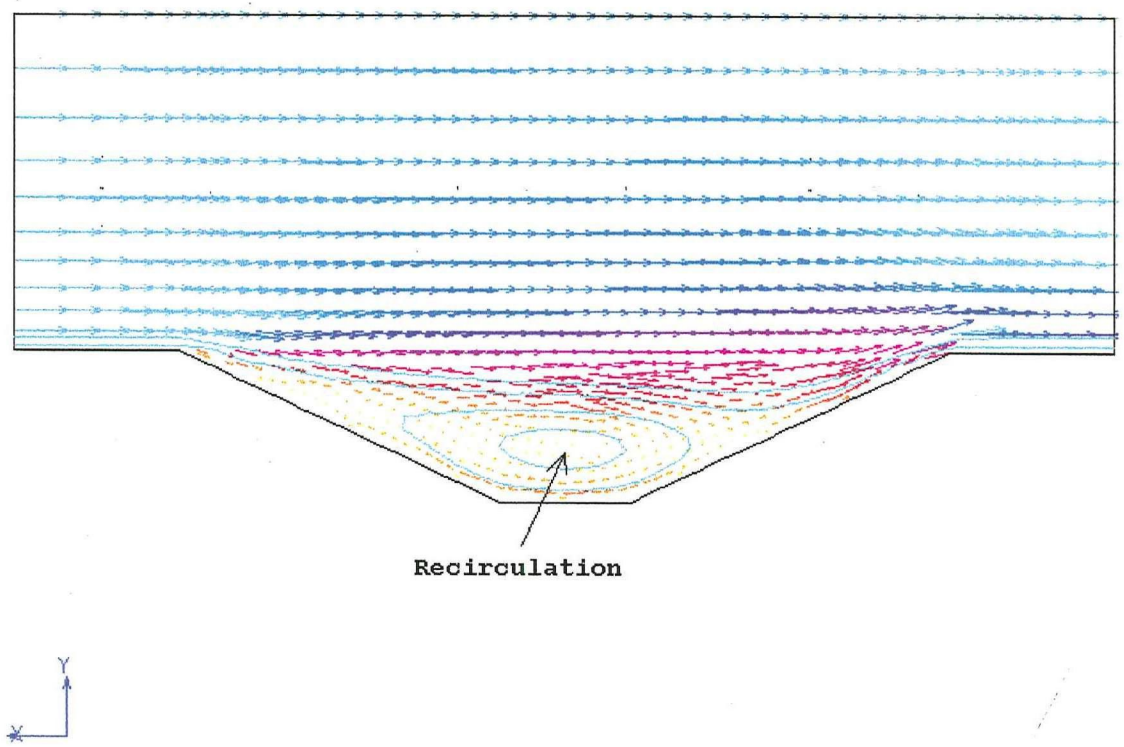

Figure 5.8 Vector and streamline plot for the trapezoidal section

S. G., et al., 1994). Since the idealized Bingham geometry can mimic the wind tunnel results, this provides additional validation of the Bingham numerical model. It should however be realized that this validation is only a qualitative one. For an idealized trapezoidal section, the emissions would escape out of the pit from the upwind side, as assumed by the ISC3 model.

5.2.3 Idealized Rectangular Geometry

The model was developed with exactly the same steps that have been discussed earlier, using a rectangular cross-section. Figures 5.9 and 5.10 illustrate the geometry/mesh plot and the wind vector/streamline plot, respectively. The dimensions of the pit were chosen so as to keep the same depth and cross-sectional area of the pit as used in the idealized trapezoidal case. Recirculation phenomenon was more pronounced here than the idealized trapezoidal shape.

5.2.4 Discussion

The exercise in this section demonstrates that the presence (or absence) of the recirculatory vortex depends on how the pit is represented. As presented, idealization of pit geometry (trapezoidal or rectangular cross-section) induces the flow separation on the upwind edge of the pit, thereby causing a recirculatory wind profile to be set up inside the mine. Since the numerical model could mimic wind tunnel results for idealized geometries

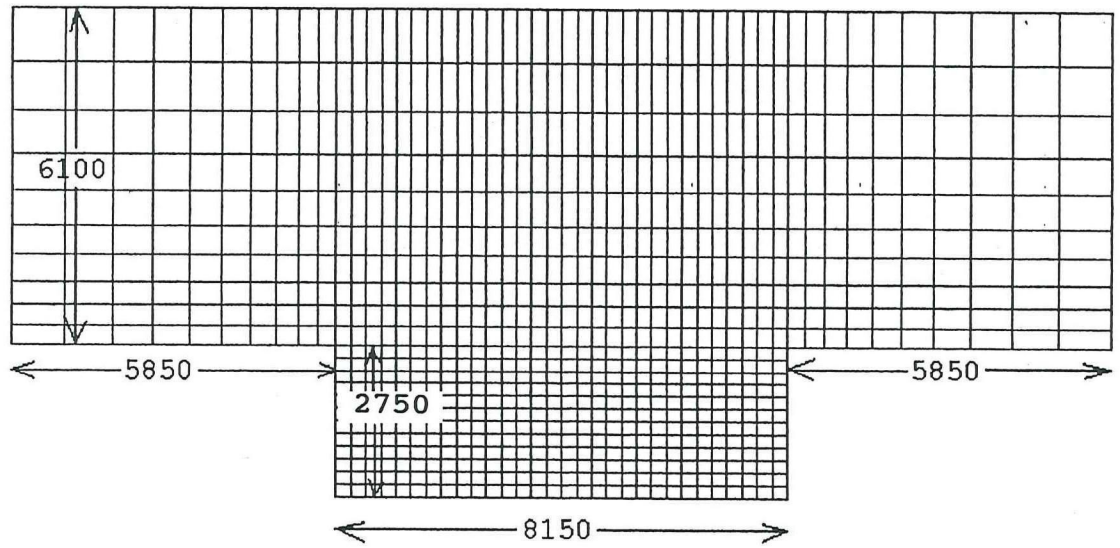

Figure 5.9 Geometry and finite element mesh for the rectangular section

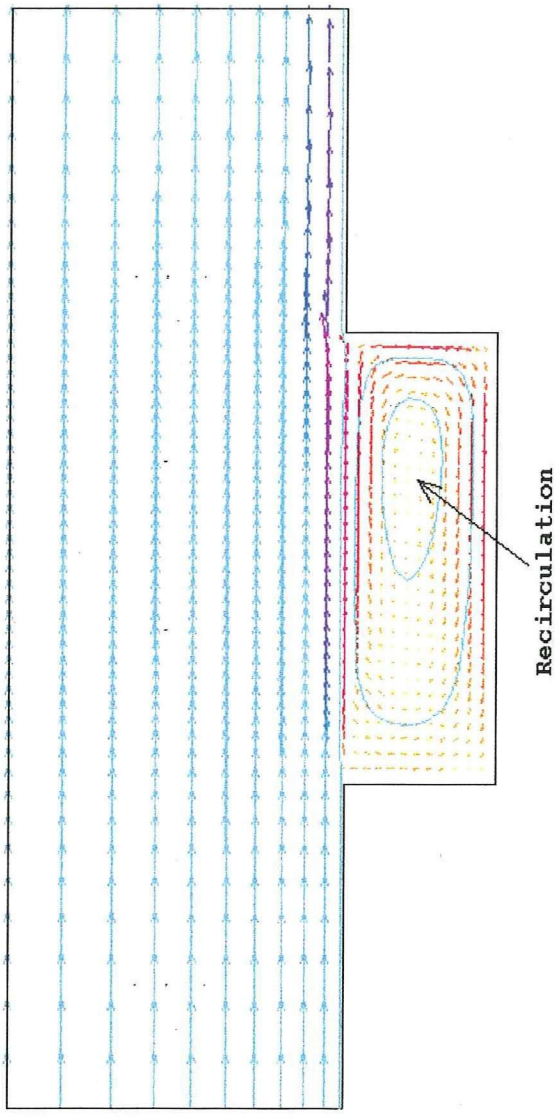

Figure 5.10 Vector and streamline plot for the rectangular section

qualitatively, it is reasonable to conclude that the model will predict airflow patterns for the "actual" pit correctly. The possible cause of the recirculatory profile being absent for the actual case is that the airflow does not encounter steep upwind edges which can induce flow separation and, hence, recirculation in the real case, at least for the Bingham pit.

CHAPTER 6

SUMMARY AND CONCLUSIONS

The purpose of the present study was to numerically simulate the turbulent diffusion, transport and pit retention of fugitive dust from the Bingham Canyon mine. A 3-dimensional finite-element numerical model was developed to meet the objectives of the study. Reynolds averaged equations, along with the κ-ϵ turbulence model and near-wall modeling approach, were used to generate the flow patterns, and the particle dispersion was subsequently simulated using a Lagrangian stochastic model. Simulation studies were conducted with the 3-dimensional numerical model to examine the sensitivity of the particle behavior (primarily pit-retention) to various meteorological and emission source parameters. The model predicted significantly lower escape fraction values for the simulations conducted in the study. Numerical tests, validation studies, and comparative analyses among different pit geometries were also performed to evaluate the performance of the Bingham pit model.

The simulations in this study exhibit realistic-looking wind patterns and particle trajectories. With some degree of accuracy, the present model can predict the

airflow and particle behavior for the Bingham pit. Unfortunately, the observational data for a direct comparison with the results of this study is not presently available. The primary aim of the present study was to provide a comparative analysis in order to understand the sensitivity of dust dispersion and retention to a wide range of parameters. Therefore, the use of data available in the literature to represent the turbulent characteristics of the atmosphere was considered appropriate.

The sensitivity analyses presented in Chapter 4 provide useful insights into the dust dispersion and pit retention phenomena for the Bingham pit as a function of the varying parameters. The results demonstrate that, generally, only a small fraction of the fugitive dust/PM-10 emitted in the Bingham Canyon mine actually leaves the boundary of the pit. The model is capable of simulating non-Gaussian dispersion and, hence, can be expected to provide results closer to real situations. However, because the analysis of 3-dimensional turbulent two-phase flows (as in this case) can be computationally expensive, the use of advanced methods such as finite-element techniques in a typical industrial setting is presently limited. Also, the increased complexity of the model demands specification of a large number of input parameters, the values of which might not be always available.

Although the model is quite useful in its present form to perform comparative simulation studies, nevertheless, several recommendations for future work and improvements are outlined below:

- In order to improve the numerical accuracy, the 3-dimensional finite element mesh should be made finer, especially near the ground level. However, it should be kept in mind that this can lead to computationally expensive calculations.
- Incorporation of the roughness features of the ground, which might spatially vary, should be investigated.
- The presence of mountainous terrain introduces significant complexities in the atmospheric transport and diffusion processes. The parameterizing of complex wind flow regimes and other turbulence parameters is a difficult task. Incorporation of these parameterizations is an area that needs further research. It is expected that use of more sophisticated and more realistic time-dependent meteorological conditions will make the predictions more accurate. Also, the use of temperature-dependent air density will increase the accuracy of the model.
- The model should be tested against the observational data, which characterizes the dust dispersion and retention phenomena based on the

meteorological and source parameters. Hi-vol samplers could be used in the field experiment study. However, this could be a challenging proposition because of the size and extent of the Bingham pit, time-dependent meteorological conditions and difficulty in isolating a particular dust source which has to be studied.

- The standard κ-ϵ model used for the present analysis is an isotropic model, which means there is no directional preference for turbulence. In order to include a more realistic scenario, the use of an anisotropic turbulence model should be investigated.
- In this study, the mixing height was chosen to be a constant value. The use of a spatially and temporally varying mixing height (top of the domain) should be investigated.
- The present study assumed that particles settle when they come in contact with the ground surface. Once settled, they cannot be resuspended. These assumptions could lead to underpredictions in estimating the value of escape fraction. The dust plume-ground interaction is an area which should be further investigated.

The preceding list represents just a few of the possibilities for future improvement of the model, which could lead to better characterization of the dust

advection, dispersion and pit retention for the Bingham Canyon mine.

The present study has demonstrated how advanced tools such as finite-element modeling can be employed to characterize the airflow patterns and pit retention of fugitive dust. There is still scope for improving the performance of the model by investigating some of the recommendations mentioned. Better parameterization of flows in complex terrain, use of field turbulence data to create model input, and testing the model against observed data are the areas on which maximum emphasis should be placed for future investigations.

APPENDIX A

"WORST" CASE SCENARIO FOR THE BINGHAM PIT

Due to Kennecott's interest in evaluating the worst-case escape fraction, Appendix A was added as a supplement.

A.1 Simulation Conditions

A simulation was generated in order to develop the worst-case escape fraction values for the Bingham pit. The conditions specified in the simulation were as follows:

Wind speed:	30 miles/hour
Wind direction:	From the south
Atmospheric stability:	Extremely Unstable (A) [This is a conservative assumption. In reality, atmosphere can only be Neutral (D) at such high wind speeds]
Source location and height:	30 feet high emission source at the north-wall [At the notch between the pit and the Bingham Canyon (TE = 2500 feet, TN = 6000 feet)]
Particle size:	PM-10

A.2 Results

Using the simulation conditions specified in section A.1, the following two cases were evaluated to quantify

the worst-case escape fraction for the Bingham pit:

- "Trap" boundary condition for the ground.
- "Ricochet" boundary condition with restitution coefficient equal to 1 for the ground.

"Trap" boundary condition signifies that particles settle when they collide with the ground. "Ricochet" boundary condition (with restitution coefficient of 1) means that particles reflect back with the same velocity as the incoming velocity on collision with the ground. Figure A.1 illustrates the particle trajectory plot for "Trap" boundary condition for the aerodynamic particle size of 10 μ. As shown in the figure, 108 trajectories (out of 500 released at the dust emission point) escape the north boundary of the domain, thereby suggesting an escape fraction of 21.6% for these test conditions.

The approximate values of the escape fractions for "Trap" and "Ricochet" conditions were calculated as 22% and 33%, respectively, for the conditions specified in Section A.1. For the "Ricochet" conditions, particles can reflect back on collision with the ground. Therefore, the value of the escape fraction for "Ricochet" boundary condition is higher than the value for the "Trap" boundary condition. Specification of "Ricochet" boundary condition at the ground is a more conservative assumption.

The simulation results demonstrate that under the worst-case conditions, about one-third of the PM-10 can escape the boundaries of the computational domain.

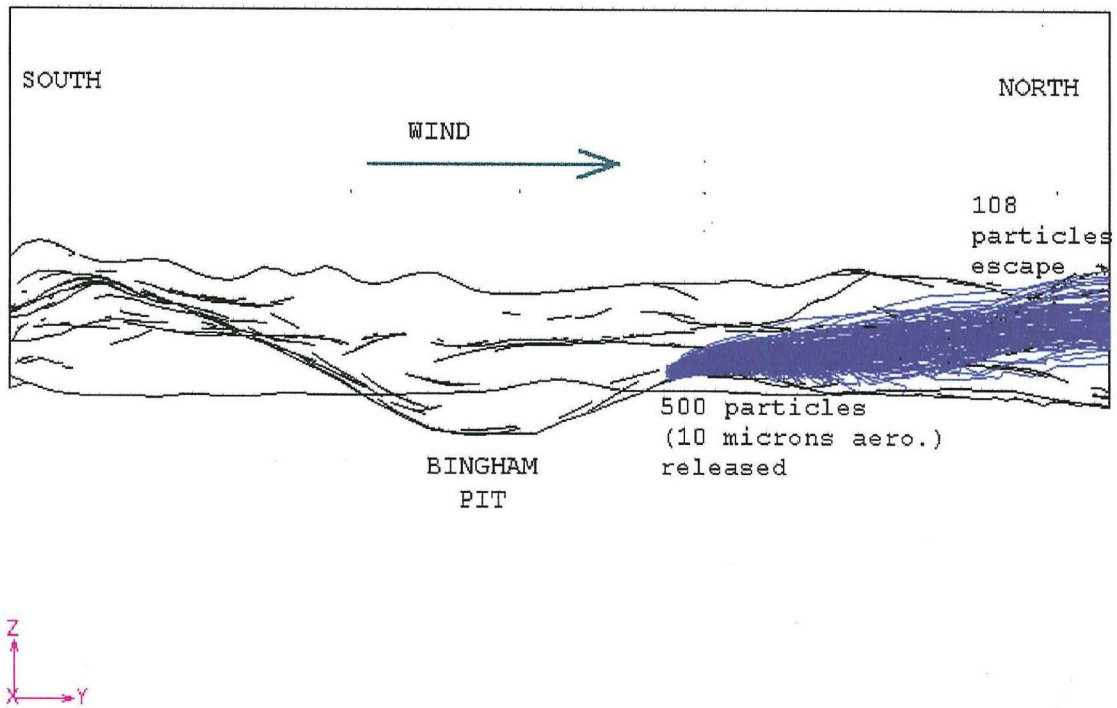

Figure A.1 Particle trajectories for the worst-case scenario ("Trap" condition)

APPENDIX B

EXAMPLE PROBLEM INPUT FILE

FOR FIDAP 7.5 RUN

```
/
/  FIPREP INPUT FILE CREATED ON 29 May 96 AT  20:50:27
/

TITLE
/ specify title

FIPREP
/ invoke the FIPREP module

 PROB (3-D, INCO, STEA, TURB, NONL, NEWT, MOME, ISOT, FIXE, SING)
 / specify equations to be solved

 EXEC (NEWJ)
 / specify mode of execution

 SOLU (SEGR = 10000, PREC = 21, ACCF = 0.000000000000E+00, NOLI, PPRO,
       SCHA = 0.000000000000E+00)
 / specify nonlinear iterative solution method

 OPTI (UPWI)
 / specify various optional equation terms

 DATA (CONT)
 / specify input data printout options

 RELA ( )
   0.8000000000E+00,  0.8000000000E+00,  0.8000000000E+00,  0.2000000000E+00,
   0.0000000000E+00,  0.0000000000E+00,  0.7000000000E+00,  0.7000000000E+00,
   0.0000000000E+00,  0.0000000000E+00,  0.0000000000E+00,  0.0000000000E+00,
   0.0000000000E+00,  0.0000000000E+00,  0.0000000000E+00,  0.0000000000E+00,
   0.0000000000E+00,  0.0000000000E+00,  0.0000000000E+00,  0.0000000000E+00,
   0.0000000000E+00,  0.0000000000E+00,  0.0000000000E+00,  0.0000000000E+00,
   0.0000000000E+00,  0.0000000000E+00,  0.0000000000E+00,  0.0000000000E+00
 / specify relaxation factors

 PRIN (NONE, BOUN)
 / specify printout time steps
```

```
ENTI (NAME = "fluid", FLUI, PROP = "air")
ENTI (NAME = "bingham", WALL, TRAP)
ENTI (NAME = "north", PLOT, ESCA)
ENTI (NAME = "south", PLOT, ESCA)
ENTI (NAME = "west", PLOT, ESCA)
ENTI (NAME = "east", PLOT, ESCA)
ENTI (NAME = "top", PLOT, RICO, REST = 1.0)
/ group various material properties and options into a single entity     definition

DENS (SET = "air", CONS = 0.625000000000E-01)
DENS (SET = "dust", CONS = 62.48)
/ specify a density model

VISC (SET = "air", CONS = 0.121000000000E-04, TWO-)
/ specify a viscosity model

BCNO (UZ, ENTI = "top", ZERO)
BCNO (UX, ENTI = "north", ZERO)
BCNO (UZ, ENTI = "north", ZERO)
BCNO (UY, ENTI = "north", CONS = -8.8)
BCNO (KINE, ENTI = "north", CONS = 3.4703)
BCNO (DISS, ENTI = "north", CONS = 0.149520000000E-01)
BCNO (VELO, ENTI = "bingham", ZERO)
/ specify constrained nodal values

ICNO (UY, CONS = -8.8, ENTI = "fluid")
ICNO (UY, CONS = -8.8, ENTI = "bingham")
ICNO (UY, CONS = -8.8, ENTI = "north")
ICNO (UY, CONS = -8.8, ENTI = "south")
ICNO (UY, CONS = -8.8, ENTI = "west")
ICNO (UY, CONS = -8.8, ENTI = "east")
ICNO (UY, CONS = -8.8, ENTI = "top")
ICNO (KINE, CONS = 3.4703, ENTI = "fluid")
ICNO (KINE, CONS = 3.4703, ENTI = "bingham")
ICNO (KINE, CONS = 3.4703, ENTI = "north")
ICNO (KINE, CONS = 3.4703, ENTI = "south")
ICNO (KINE, CONS = 3.4703, ENTI = "west")
ICNO (KINE, CONS = 3.4703, ENTI = "east")
ICNO (KINE, CONS = 3.4703, ENTI = "top")
ICNO (DISS, CONS = 0.149520000000E-01, ENTI = "fluid")
ICNO (DISS, CONS = 0.149520000000E-01, ENTI = "bingham")
ICNO (DISS, CONS = 0.149520000000E-01, ENTI = "north")
ICNO (DISS, CONS = 0.149520000000E-01, ENTI = "south")
ICNO (DISS, CONS = 0.149520000000E-01, ENTI = "west")
ICNO (DISS, CONS = 0.149520000000E-01, ENTI = "east")
ICNO (DISS, CONS = 0.149520000000E-01, ENTI = "top")
/ specify initial nodal values for the various degrees of freedom

CLIP (MINI)
 0.0000000000E+00,  0.0000000000E+00,  0.0000000000E+00,  0.0000000000E+00,
```

```
  0.0000000000E+00,  0.0000000000E+00,  0.1000000000E-19,  0.1000000000E-24,
  0.0000000000E+00,  0.0000000000E+00,  0.0000000000E+00,  0.0000000000E+00,
  0.0000000000E+00,  0.0000000000E+00,  0.0000000000E+00,  0.0000000000E+00,
  0.0000000000E+00,  0.0000000000E+00,  0.0000000000E+00,  0.0000000000E+00,
  0.0000000000E+00,  0.0000000000E+00,  0.0000000000E+00,  0.0000000000E+00,
  0.0000000000E+00,  0.0000000000E+00,  0.0000000000E+00,  0.0000000000E+00
 / specify upper and lower bounds for any degree of freedom

END
/ terminate execution
```

REFERENCES

1. Azad, R.S. The Atmospheric Boundary Layer for Engineers. Kluwer Academic Publishers, Netherlands, 1993.

2. Chan, S.T., Gresho, P.M. and Lee, R.L. Simulation of LNG vapour spread and dispersion by finite element methods. Appl. Math. Modelling. Vol. 4, 1980, pp. 335-344.

3. Clift, R., Grace, J.R. and Weber, M.E. Bubbles, Drops and Particles. Academic Press, New York, 1978.

4. Costa, M.J., Riethmuller, M.L. and Borrego, C. Wind-tunnel simulation of gas dispersion over complex terrain: comparison of two length-scale studies. Atmospheric Environment. Vol. 28, No. 11, 1994, pp. 1933-1938.

5. Csanady, G.T. Turbulent diffusion in the environment. D. Reidel Publishing Company, Boston, 1972.

6. DeNevers, N. Air Pollution Control Engineering. McGraw-Hill, New York, 1995.

7. Draxler, R.R. and Heffter, J.L. Workbook for estimating the climatology of regional-continental scale atmospheric dispersion and deposition over the United States. NOAA Technical Memorandum ERL ARL-96, Air Resources Laboratories, Silver Spring, Maryland, 1981.

8. Egan, B.A. Dispersion in Complex Terrain: A report of a Workshop held at Keystone, Colorado, May 17-20, 1983. EPA/600/S9-85/031, U.S. EPA, NC, 1986.

9. Elghobashi, S. On predicting particle-laden turbulent flows. Applied Scientific Research. Vol. 52, 1994, pp. 309-329.

10. Environmental Protection Agency, 1994: Modeling fugitive dust impacts from surface coal mining operations-phase II. EPA-454/R-94-025, U.S. EPA, Research Triangle Park, NC.

11. Environmental Protection Agency, 1995: User's guide for the Industrial Source Complex (ISC3) dispersion models - Vol. I and II. EPA-454/B-95-003a and EPA-454/B-95-003b, U.S. EPA, Research Triangle Park, NC.

12. Fluid Dynamics International, Inc. Users manuals for FIDAP 7.0 and 7.5, 1993 and 1995, FDI, Evanston, IL.

13. Gosman, A.D. and Ioannides, E. Aspects of computer simulation of liquid-fuelled combustors. AIAA 19th Aerospace Science Mtg., Paper No. 81-0323, St. Louis, MO, 1981.

14. Hanna, S.R., Briggs, G.A. and Hosker, R.P. Handbook on Atmospheric Diffusion, DOE/TIC-11223, Technical Information Center, 1982.

15. Haroutunian, V. and Engelman, M.S. On modeling wall-bound turbulent flows using specialized near-wall finite elements and the standard κ-ϵ turbulence model. Advances in numerical simulation of turbulent flows, FED - Vol. 117, ASME 1991.

16. Haroutunian, V. and Engelman, M.S. Two-equation simulations of turbulent flows: a commentary on physical and numerical aspects. Advances in finite element analysis in fluid dynamics, FED - Vol. 171, ASME 1993.

17. Herwehe, J.A. Numerical modeling of turbulent diffusion of fugitive dust from an idealized open-pit mine. MS Thesis, Iowa State University, Ames, Iowa, 1984.

18. Hinds, W.C. Aerosol Technology. John Wiley & Sons, USA, 1982.

19. Kennecott Utah Copper, Bingham Canyon mine emission inventory, 1994.

20. Khurshudyan, L.H., Snyder, W.H. and Nekrasov, I.V. Flow and dispersion of pollutants over two-dimensional hills: summary report on joint Soviet-American study. EPA-600/S4-81-067, US. EPA, NC, 1982.

21. Launder, B.E. and Spalding, D.B. The numerical computation of turbulent flows. Comp. in Applied Mech. and Engng. Vol. 3, 1974, pp. 269-289.

22. Lee, Hsi-nan. Finite element solution to equations for turbulent motion and diffusion in planetary boundary layer. Ph.D. Dissertation, University of

Utah, Utah, 1977.

23. McBean, G.A., et al. The Planetary Boundary Layer. Technical note no. 165, World Meteorological Organization, Geneva, Switzerland, 1979.

24. Nallasamy, M. A critical evaluation of various turbulence models as applied to internal fluid flows. Technical paper 2474, NASA, 1985.

25. National Oceanic and Atmospheric Administration, Local Climatological Data, Salt Lake City, UT, 1991-1994.

26. Ormancey, A. and Martinon, J. Prediction of particle dispersion in turbulent flows. PCH PhysicoChemical Hydrodynamics. Vol. 5, 1984, pp. 229-244.

27. Panchev, S. Dynamic Meteorology. D Reidel Publishing Company, Netherlands, 1985.

28. Panofsky, H.A. Tower Micrometeorology. Workshop on Micrometeorology, American Meteorological Society, 1973.

29. Panofsky, H.A. A model for vertical diffusion coefficients in a growing urban boundary layer. Boundary-Layer Meteorology. Vol. 9, 1975, pp. 235-244.

30. Panofsky, H.A. and Dutton, J.A. Atmospheric Turbulence. John Wiley & Sons, USA, 1984.

31. Perdikaris, G.A. and Mayinger, F. Numerical simulation of the spreading of buoyant gases over topographically complex terrain. International Journal of Energy Research. Vol. 19, 1995, pp. 53-61.

32. Perry, S.G., Thompson, R.S. and Peterson, W.B. Considerations for modeling small-particulate impacts from surface coal-mining operations based on wind-tunnel simulations. American Meteorological Society - Eighth Joint Conference on the applications of air pollution meteorology with the AWMA, 23-28 January, 1994, Nashville.

33. Rodi, W. Turbulence models and their application in hydraulics - a state of the art review. IAHR, Netherlands, 1984.

34. Snyder, W.H. Guideline for fluid modeling of atmospheric diffusion. EPA-600/8-81-009, U.S. EPA,

NC, 1981.

35. Thompson, R.S. Residence time of contaminants released in surface coal mines - a wind-tunnel study. American Meteorological Society - Eighth Joint Conference on the applications of air pollution meteorology with the AWMA, 23-28 January, 1994, Nashville.

36. TRC Environmental Consultants, Inc. Dispersion of airborne particulates in surface coal mines - data analysis. EPA-450/4-85-001, U.S. EPA, NC, 1985.

37. TRC Environmental Consultants, Inc. Continued analysis and derivation of a method to model pit retention. EPA-450/4-86-003, U.S. EPA, NC, 1986.

38. Wall, S., John, W., Wang, H. and Goren, S.L. Measurements of kinetic energy loss for particles impacting surfaces. Aerosol Science and Technology. Vol. 12, 1990, pp. 926-946.

39. Yu, Tsann-Wang. A comparative study on parameterization of vertical turbulent exchange processes. Monthly Weather Review. Vol. 105, January 1977, pp. 57-66.

40. Zannetti, P. Air Pollution Modeling. Van Nostrand Reinhold, New York, 1990.

41. Zhang, Y.Q., Huber, A.H., Arya, S.P.S. and Snyder, W.H. Numerical simulation to determine the effects of incident wind shear and turbulence level on the flow around a building. Journal of Wind Engineering and Industrial Aerodynamics. 46 & 47, 1993, pp. 129-134.